Available online at www.sciencedirect.com
ScienceDirect
Comput. Methods Appl. Mech. Engrg. 304 (2016) 501–520
Computer methods in applied mechanics and engineering
www.elsevier.com/locate/cma

Modeling and analysis of the optical black hole in metamaterials by the finite element time-domain method[☆]

Wei Yang[a], Jichun Li[b,*], Yunqing Huang[a]

[a] Hunan Key Laboratory for Computation and Simulation in Science and Engineering, Xiangtan University, China
[b] Department of Mathematical Sciences, University of Nevada Las Vegas, Las Vegas, NV 89154-4020, USA

Received 2 October 2015; received in revised form 21 February 2016; accepted 22 February 2016
Available online 4 March 2016

Abstract

In this paper we propose a finite element time-domain method for modeling the optical black holes (OBHs) coupled with the perfectly matched layer (PML) technique. Stability analysis is carried out for the proposed scheme. Simulations of cylindrical, elliptical and square black holes demonstrate that our method is quite effective in modeling OBHs in time domain. To our best knowledge, this is the first OBHs simulation realized by the finite element time-domain method.

MSC: 78M10; 65N30; 65F10; 78-08

Keywords: Optical black holes; Finite element method; Maxwell's equations; Edge element

1. Introduction

In 2000, the metamaterials with negative refraction index were successfully constructed. Since then metamaterials have been a very hot research topic due to its many potential applications, such as invisible cloaks (cf. [1,2]), electromagnetic absorbers [3], electrically small resonators, waveguides that can go beyond the diffraction limit, perfect lens, and subwavelength imaging. Details on metamaterials can be found in many recently published monographs (e.g., [4–7]). In 2009, based on metamaterial structures, Narimanov and Kildishev [3] proposed an approach for broad-band omnidirectional electromagnetic wave absorption. The devices designed by them are called the optical black holes (OBHs), which can efficiently absorb the wave coming from all directions, including wave scattered from the natural environment. Such OBHs can find many potential applications in photovoltaics, solar energy harvesting, and optoelectronics.

☆ Work partially supported by NSFC Project 11401506, NSFC Project 11271310, NSFC Key Project 11031006, National Science Foundation grant DMS-1416742, and Hunan Education Department Project (15B236).
* Corresponding author.
E-mail addresses: yangweixtu@126.com (W. Yang), jichun@unlv.nevada.edu (J. Li), huangyq@xtu.edu.cn (Y. Huang).

http://dx.doi.org/10.1016/j.cma.2016.02.029

Numerical simulations of OBHs play a very important role in seeking new designs and theoretical predictions. Due to its simplicity, the finite difference time domain (FDTD) method is one of the most popular techniques used for electromagnetic wave propagation simulation in general media and metamaterials [8]. For example, Argyropoulos et al. [9] demonstrated the excellent absorption for spherical OBHs using a radially dependent FDTD simulation technique. Qiu et al. [10] studied the radiative properties of optical board periodically embedded with OBHs with the FDTD method. However, the FDTD method is also famous for the staircase effect when dealing problems with complex geometries [8,11]. In these cases, engineers and physicists often resort to the popular commercial finite element based multiphysics package COMSOL. However, COMSOL is very inefficient in solving time dependent Maxwell's equations. Hence developing efficient finite element time-domain (FETD) methods plays a very important role in simulating wave propagation in general media and metamaterials.

Though there exist many excellent works on finite element methods for solving Maxwell's equations in various media (e.g., papers [12–24,11], books [25–28] and references cited therein), to our best knowledge, we are unaware of any FETD methods developed for simulating OBHs. In this paper, we extend our recent efforts on developing FETD methods for metamaterials (e.g., [7,29,30]) to solve the two-dimensional (2D) OBHs. Specifically, we first derive the modeling equations and prove the stability. Then we develop a FETD algorithm to simulate the wave absorbing phenomenon for OBHs.

The rest of the paper is organized as follows. In Section 2, we present the governing equations for the OBHs and the perfectly matched layer (PML). Then we prove the stability of the modeling equations. In Section 3, we develop a FETD scheme with edge elements to solve our modeling equations. A discrete stability for the scheme is proved. Then in Section 4, many interesting simulations of cylindrical, elliptical and square black holes by our FETD method are provided. Finally, we conclude the paper in Section 5.

2. Governing equations of the OBHs

The modeling of the optical black hole is based on Faraday's Law and Ampere's Law, which are written as follows:

$$\frac{\partial \boldsymbol{B}}{\partial t} = -\nabla \times \boldsymbol{E}, \tag{2.1}$$

$$\frac{\partial \boldsymbol{D}}{\partial t} = \nabla \times \boldsymbol{H}, \tag{2.2}$$

and the constitutive relations

$$\boldsymbol{D} = \varepsilon_0 \varepsilon_r \boldsymbol{E}, \tag{2.3}$$

$$\boldsymbol{B} = \mu_0 \mu_r \boldsymbol{H}, \tag{2.4}$$

where $\boldsymbol{E}$ and $\boldsymbol{H}$ are the electric and magnetic fields, respectively, $\boldsymbol{D}$ and $\boldsymbol{B}$ are the electric displacement and magnetic induction, respectively, ε_r and μ_r are the relative electric permittivity and magnetic permeability, respectively, and ε_0 and μ_0 are the electric permittivity and magnetic permeability in vacuum, respectively.

Let us first consider a two-dimensional (2D) cylindrical optical black holes. This device is divided into two regions: the shell region is used to change the direction of wave propagation, and the core region is usually used to absorb the wave. The radially dependent electric permittivity distribution of the cylindrical black holes was proposed by Narimanov and Kildishev [3]:

$$\varepsilon_r(r) = \begin{cases} \varepsilon_1, & r > R_s \\ \varepsilon_1 \left(\dfrac{R_s}{r}\right)^n, & R_c \le r \le R_s \\ \varepsilon_2 + i\gamma & r < R_c, \end{cases} \tag{2.5}$$

where ε_1 is the relative electric permittivity of the surrounding medium, $\varepsilon_2 > \varepsilon_1$ is the relative electric permittivity of the core, $\gamma > 0$ is the loss, n is a positive integer, r is the radial distance from the center of the black hole, and R_s and R_c are the radii of the shell and core of the black hole, respectively. To reduce the reflection of the electromagnetic waves, R_c is chosen to satisfy the identity

$$R_c = R_s \sqrt[n]{\frac{\varepsilon_1}{\varepsilon_2}}.$$

In [3], Narimanov used the semiclassical transformation optics to design the metamaterials which can collect the light from all directions, including light scattered from the natural environment. One advantage of the optical black hole is that it can be realized by existing ordinary materials. From (2.5), we can see that the real part of the relative electric permittivity ε_r is larger than one. Note that the relative magnetic permeability μ_r is equal to one for ordinary media. Since the electric permittivity is complex-valued, the current density

$$\boldsymbol{J} = \sigma \boldsymbol{E},$$

should be added to Eqs. (2.2), where $\sigma = \omega \cdot Im(\varepsilon_r) \cdot \varepsilon_0 = 2\pi f \cdot Im(\varepsilon_r) \cdot \varepsilon_0$ is the conductivity, and f is the operating frequency. Hence we can obtain the governing equations of the optical black hole: Find $\boldsymbol{E} = (E_x, E_y)'$ and $H = H_z$ satisfy

$$\mu_0 \frac{\partial H}{\partial t} = -\nabla \times \boldsymbol{E}, \tag{2.6}$$

$$\varepsilon_0 Re(\varepsilon_r) \frac{\partial \boldsymbol{E}}{\partial t} + \sigma \boldsymbol{E} = \nabla \times H. \tag{2.7}$$

For simplicity, here and below we use the 2D curls $\nabla \times \boldsymbol{E} = \frac{\partial E_y}{\partial x} - \frac{\partial E_x}{\partial y}$ and $\nabla \times H = (\frac{\partial H}{\partial y}, -\frac{\partial H}{\partial x})'$.

To model OBHs, we have to reduce an unbounded physical domain to a bounded domain. Here we use the perfectly matched layer (PML) technique to absorb waves leaving the computational domain without introducing reflections. The governing equations of the two dimensional Berenger's split PML can be written as [31]: In the PML region Ω_{pml},

$$\varepsilon_0 \varepsilon_1 \frac{\partial E_x}{\partial t} + \sigma_y E_x = \frac{\partial H_z}{\partial y}, \tag{2.8}$$

$$\varepsilon_0 \varepsilon_1 \frac{\partial E_y}{\partial t} + \sigma_x E_y = -\frac{\partial H_z}{\partial x}, \tag{2.9}$$

$$\mu_0 \frac{\partial H_{zx}}{\partial t} + \sigma_{mx} H_{zx} = -\frac{\partial E_y}{\partial x}, \tag{2.10}$$

$$\mu_0 \frac{\partial H_{zy}}{\partial t} + \sigma_{my} H_{zy} = \frac{\partial E_x}{\partial y}, \tag{2.11}$$

where the original magnetic field H_z is split into two components, i.e., $H_z = H_{zx} + H_{zy}$. Here the parameters σ_i and σ_{mi} $(i = x, y)$ are homogeneous to the electric and magnetic conductivities in the x and y directions, respectively.

Now we combine the governing equations in both the PML region and the black hole region into a unified form:

$$\varepsilon_0 \varepsilon_r^* \frac{\partial \boldsymbol{E}}{\partial t} + \sigma^* \boldsymbol{E} = \nabla \times H_z, \tag{2.12}$$

$$\mu_0 \frac{\partial H_{zx}}{\partial t} + \sigma_{mx}^* H_{zx} = -\frac{\partial E_y}{\partial x}, \tag{2.13}$$

$$\mu_0 \frac{\partial H_{zy}}{\partial t} + \sigma_{my}^* H_{zy} = \frac{\partial E_x}{\partial y}, \tag{2.14}$$

where

$$\sigma^* = \begin{cases} \begin{bmatrix} \sigma & 0 \\ 0 & \sigma \end{bmatrix} & \text{in } \Omega_c, \\ \begin{bmatrix} \sigma_y & 0 \\ 0 & \sigma_x \end{bmatrix} & \text{in } \Omega_{pml}, \end{cases} \qquad \varepsilon_r^* = \begin{cases} Re(\varepsilon_r), & \text{in } \Omega_c \\ \varepsilon_1, & \text{in } \Omega_{pml}, \end{cases} \qquad \sigma_{m,i}^* = \begin{cases} 0, & \text{in } \Omega_c, \\ \sigma_{m,i}, & \text{in } \Omega_{pml}, \end{cases} \qquad (i = x, y),$$

where Ω_c denotes the black hole region and the surrounding medium region (cf. Fig. 2.1).

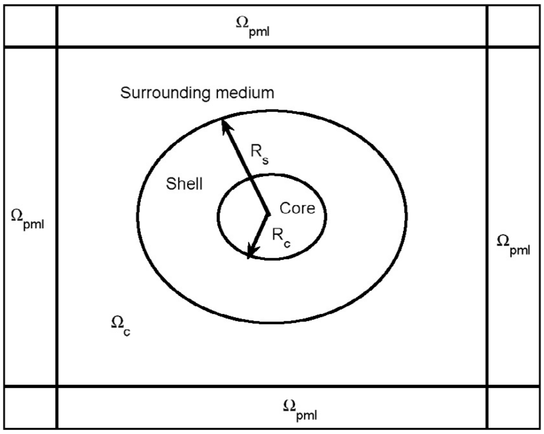

Fig. 2.1. The setup of the optical black hole model.

For simplicity, we assume that the boundary of $\Omega = \overline{\Omega_c} \cup \Omega_{pml}$ is perfectly conducting so that

$$\boldsymbol{n} \times \boldsymbol{E} = \boldsymbol{0}, \quad \text{on } \partial\Omega, \tag{2.15}$$

where $\boldsymbol{n}$ is the unit outward normal to $\partial\Omega$, and the initial conditions for the system (2.12)–(2.14) are assumed to be

$$\boldsymbol{E}(\boldsymbol{x},0) = \boldsymbol{E}_0(\boldsymbol{x}), \qquad H_{zx}(\boldsymbol{x},0) = H_{x0}(\boldsymbol{x}), \qquad H_{zy}(\boldsymbol{x},0) = H_{y0}(\boldsymbol{x}),$$

where $\boldsymbol{E}_0$, H_{x0}, H_{y0} are some given functions.

Denote $k_1 = \frac{\sigma^*_{mx}}{\mu_0}$, $k_2 = \frac{\sigma^*_{my}}{\mu_0}$. Under the assumption that σ^*_{mx} is independent of t, we can solve H_{zx} from (2.13) to have

$$H_{zx}(x,t) = H_{x0}e^{-k_1 t} + \frac{1}{\mu_0}\int_0^t \left(-\frac{\partial E_y}{\partial x}\right) e^{-k_1(t-s)} ds. \tag{2.16}$$

Similarly, solving H_{zy} from (2.14), we have

$$H_{zy}(x,t) = H_{y0}e^{-k_2 t} + \frac{1}{\mu_0}\int_0^t \left(\frac{\partial E_x}{\partial y}\right) e^{-k_2(t-s)} ds. \tag{2.17}$$

Substituting (2.16) and (2.17) into (2.12), we have

$$\varepsilon_0\mu_0\varepsilon_r^* \frac{\partial^2 \boldsymbol{E}}{\partial t^2} + \sigma^* \frac{\partial \boldsymbol{E}}{\partial t} + \nabla \times \nabla \times \boldsymbol{E} + \nabla \times \boldsymbol{S} = 0, \tag{2.18}$$

where we denote

$$\boldsymbol{S} = \sigma^*_{mx} H_{x0}e^{-k_1 t} + \sigma^*_{my} H_{y0}e^{-k_2 t} + \int_0^t \left(-\frac{\partial E_y}{\partial x}\right) e^{-k_1(t-s)} ds + \int_0^t \left(\frac{\partial E_x}{\partial y}\right) e^{-k_2(t-s)} ds.$$

Now we can form a weak formulation of (2.18): Find $\boldsymbol{E} \in H_0(curl;\Omega)$ such that

$$\varepsilon_0\mu_0 \left(\varepsilon_r^* \frac{\partial^2 \boldsymbol{E}}{\partial t^2}, \boldsymbol{\phi}\right) + \left(\sigma^* \frac{\partial \boldsymbol{E}}{\partial t}, \boldsymbol{\phi}\right) + (\nabla \times \boldsymbol{E}, \nabla \times \boldsymbol{\phi}) + (\boldsymbol{S}, \nabla \times \boldsymbol{\phi}) = 0, \tag{2.19}$$

holds true for any $\boldsymbol{\phi} \in H_0(curl;\Omega)$. The governing equation (2.19) is a vector wave integro-differential equation involving just one unknown $\boldsymbol{E}$, which can be used for the three dimensional simulation. But developing a fully discrete finite element scheme for (2.19) is quite complicated (cf. [7]), below we will design a simpler and more effective finite element scheme for the 2D OBHs.

The original split PML (2.8)–(2.11) was found to be only weakly well posed, and it may suffer explosive instability for long time simulations [32]. Hence, here we use an unsplit PML for our OBHs simulation [29]:

$$\varepsilon_0\varepsilon_r^*\frac{\partial \boldsymbol{E}}{\partial t}+\sigma^*\boldsymbol{E}=\nabla\times H_z, \tag{2.20}$$

$$\mu_0\frac{\partial H_z}{\partial t}+\left(\sigma_{mx}^*+\sigma_{my}^*\right)H_z+\nabla\times\boldsymbol{E}+\sigma_{mx}^*\sigma_{my}^*Q_z+\sigma_{my}^*\frac{\partial P_y}{\partial x}-\sigma_{mx}^*\frac{\partial P_x}{\partial y}=0, \tag{2.21}$$

$$\mu_0\frac{\partial \boldsymbol{P}}{\partial t}=\boldsymbol{E}, \tag{2.22}$$

$$\mu_0\frac{\partial Q_z}{\partial t}=H_z. \tag{2.23}$$

This model was developed in our previous work [29], and $\boldsymbol{P}=(P_x,P_y)'$ and Q_z are auxiliary variables.

Taking the time derivative of (2.21), and substituting (2.22) and (2.23) into (2.21), we have

$$\varepsilon_0\varepsilon_r^*\frac{\partial \boldsymbol{E}}{\partial t}+\sigma^*\boldsymbol{E}=\nabla\times H_z, \tag{2.24}$$

$$\mu_0\frac{\partial^2 H_z}{\partial t^2}+\left(\sigma_{mx}^*+\sigma_{my}^*\right)\frac{\partial H_z}{\partial t}+\frac{\sigma_{mx}^*\sigma_{my}^*}{\mu_0}H_z+\nabla\times\frac{\partial \boldsymbol{E}}{\partial t}+\nabla\times\boldsymbol{E}^*=0, \tag{2.25}$$

where $\boldsymbol{E}^*=(k_1E_x,k_2E_y)'$.

The weak formulation of Eqs. (2.24)–(2.25) can be written as follows: find $\boldsymbol{E}\in H_0(curl;\Omega)$, $H_z\in L^2(\Omega)$ such that

$$\varepsilon_0\left(\varepsilon_r^*\frac{\partial \boldsymbol{E}}{\partial t},\boldsymbol{\phi}\right)+(\sigma^*\boldsymbol{E},\boldsymbol{\phi})=(H_z,\nabla\times\boldsymbol{\phi}), \tag{2.26}$$

$$\mu_0\left(\frac{\partial^2 H_z}{\partial t^2},\varphi\right)+\left((\sigma_{mx}^*+\sigma_{my}^*)\frac{\partial H_z}{\partial t},\varphi\right)+\left(\frac{\sigma_{mx}^*\sigma_{my}^*}{\mu_0}H_z,\varphi\right)+\left(\nabla\times\left(\frac{\partial \boldsymbol{E}}{\partial t}+\boldsymbol{E}^*\right),\varphi\right)=0, \tag{2.27}$$

hold true for any $\boldsymbol{\phi}\in H_0(curl;\Omega)$, and $\varphi\in L^2(\Omega)$.

Next, we will give a stability result for the problem (2.26)–(2.27).

Theorem 2.1. *For the solution of (2.26)–(2.27), the following stability holds true:*

$$\left\|\frac{\partial H_z}{\partial t}(t)\right\|_0^2+\left\|\sqrt{\sigma_{mx}^*\sigma_{my}^*}H_z(t)\right\|_0^2+\left\|\frac{\partial \boldsymbol{E}}{\partial t}(t)\right\|_0^2+\|\nabla\times H_z(t)\|_0^2+\|\boldsymbol{E}(t)\|_0^2\le CF(0), \tag{2.28}$$

where $C>0$ is a constant, and the function $F(0)$ depends on initial conditions $H_z(0),\boldsymbol{E}(0)$, $\frac{\partial \boldsymbol{E}}{\partial t}(0)$, $\frac{\partial H_z}{\partial t}(0)$ and $\nabla\times H_z(0)$. Here and below we denote $\|\boldsymbol{E}(t)\|_0^2=\|E_x\|_0^2+\|E_y\|_0^2$. Similar notation is used for L^2 norm of other vectors such as $\frac{\partial \boldsymbol{E}}{\partial t}(t)$.

Proof. Choosing $\varphi=\frac{\partial H_z}{\partial t}$ in (2.27), and noting that σ_{mx}^* and $\sigma_{my}^*\ge 0$, we obtain

$$\mu_0\left(\frac{\partial^2 H_z}{\partial t^2},\frac{\partial H_z}{\partial t}\right)+\left(\frac{\sigma_{mx}^*\sigma_{my}^*}{\mu_0}H_z,\frac{\partial H_z}{\partial t}\right)+\left(\nabla\times\frac{\partial \boldsymbol{E}}{\partial t},\frac{\partial H_z}{\partial t}\right)+\left(\nabla\times\boldsymbol{E}^*,\frac{\partial H_z}{\partial t}\right)\le 0. \tag{2.29}$$

Using the fact that $\varepsilon_1\le\varepsilon_r^*\le\varepsilon_2$, and choosing $\boldsymbol{\phi}=\frac{\partial \boldsymbol{E}}{\partial t}$ in the time derivative of (2.26), $\nabla\times\frac{\partial H_z}{\partial t}$ and $\boldsymbol{E}$ in (2.26), respectively, we have

$$\frac{\varepsilon_0}{2}\left(\varepsilon_r^*\frac{\partial^2 \boldsymbol{E}}{\partial t^2},\frac{\partial \boldsymbol{E}}{\partial t}\right)\le\frac{1}{2}\left(\nabla\times\frac{\partial H_z}{\partial t},\frac{\partial \boldsymbol{E}}{\partial t}\right), \tag{2.30}$$

$$\left(\frac{1}{2\varepsilon_0\varepsilon_r^*}\nabla\times\frac{\partial H_z}{\partial t},\nabla\times H_z\right)=\frac{1}{2}\left(\boldsymbol{E}_t,\nabla\times\frac{\partial H_z}{\partial t}\right)+\left(\frac{\sigma^*}{2\varepsilon_0\varepsilon_r^*}\boldsymbol{E},\nabla\times\frac{\partial H_z}{\partial t}\right), \tag{2.31}$$

$$4\varepsilon_0\varepsilon_1\varepsilon_2 C_x^2\left(\frac{\partial \boldsymbol{E}}{\partial t}, \boldsymbol{E}\right) \le 4\varepsilon_2 C_x^2(\nabla\times H_z, \boldsymbol{E}), \tag{2.32}$$

where the constant $C_x = \max(\gamma\omega, C_p)$, and $C_p = \max_{\overline{\Omega}}(\frac{\sigma^*_{mx}}{\mu_0}, \frac{\sigma^*_{my}}{\mu_0})$.

Summing up (2.29)–(2.32), and integrating the resultant over $[0, t]$, we obtain

$$\begin{aligned}
&\frac{\mu_0}{2}\left\|\frac{\partial H_z}{\partial t}(t)\right\|_0^2 + \frac{1}{2\mu_0}\left\|\sqrt{\sigma^*_{mx}\sigma^*_{my}}H_z(t)\right\|_0^2 + \frac{\varepsilon_0\varepsilon_1}{4}\|\boldsymbol{E}_t(t)\|_0^2 + \frac{1}{4\varepsilon_0\varepsilon_2}\|\nabla\times H_z(t)\|_0^2 + 4\varepsilon_0\varepsilon_1\varepsilon_2C_x^2\|\boldsymbol{E}(t)\|_0^2\\
&\quad\le \boldsymbol{g}(0) - \int_0^t\left(\boldsymbol{E}^*, \nabla\times\frac{\partial H_z}{\partial t}\right)dt + \int_0^t\left(\frac{\sigma^*}{2\varepsilon_0\varepsilon_r^*}\boldsymbol{E}, \nabla\times\frac{\partial H_z}{\partial t}\right)dt + 4\varepsilon_2C_x^2\int_0^t(\nabla\times H_z, \boldsymbol{E})dt,
\end{aligned}\tag{2.33}$$

where

$$\begin{aligned}
\boldsymbol{g}(0) &= \frac{\mu_0}{2}\left\|\frac{\partial H_z}{\partial t}(0)\right\|_0^2 + \frac{1}{2\mu_0}\left\|\sqrt{\sigma^*_{mx}\sigma^*_{my}}H_z(0)\right\|_0^2 + \frac{\varepsilon_0\varepsilon_2}{4}\|\boldsymbol{E}_t(0)\|_0^2\\
&\quad + \frac{1}{4\varepsilon_0\varepsilon_1}\|\nabla\times H_z(0)\|_0^2 + 4\varepsilon_0\varepsilon_1\varepsilon_2C_x^2\|\boldsymbol{E}(0)\|_0^2.
\end{aligned}$$

Using integration by parts, we have

$$\begin{aligned}
\int_0^t\left(\boldsymbol{E}^*, \nabla\times\frac{\partial H_z}{\partial t}\right) &= \int_\Omega\int_0^t \boldsymbol{E}^*\frac{d}{dt}\nabla\times H_z\\
&= \left(\nabla\times H_z(t), \frac{\partial \boldsymbol{E}^*}{\partial t}(t)\right) - (\nabla\times H_z(0), \boldsymbol{E}^*(0)) - \int_0^t\left(\frac{\partial \boldsymbol{E}^*}{\partial t}, \nabla\times H_z\right)dt\\
&\le \left(\nabla\times H_z(t), \frac{\partial \boldsymbol{E}^*}{\partial t}(t)\right) - (\nabla\times H_z(0), \boldsymbol{E}^*(0)) + \frac{C_x}{2}\int_0^t\left\|\frac{\partial \boldsymbol{E}}{\partial t}\right\|_0^2 + \frac{C_x}{2}\int_0^t\|\nabla\times H_z\|_0^2.
\end{aligned}$$

It is easy to see that

$$(\nabla\times H_z(0), \boldsymbol{E}^*(0)) \le \frac{C_x}{2}\|\boldsymbol{E}(0)\|_0^2 + \frac{C_x}{2}\|\nabla\times H_z(0)\|_0^2,$$

and

$$\begin{aligned}
(\nabla\times H_z(t), \boldsymbol{E}^*(t)) &\le \delta_1\varepsilon_0\|\boldsymbol{E}^*(t)\|_0^2 + \frac{1}{4\varepsilon_0\delta_1}\|\nabla\times H_z(t)\|_0^2\\
&\le \delta_1\varepsilon_0C_x^2\|\boldsymbol{E}(t)\|_0^2 + \frac{1}{4\varepsilon_0\delta_1}\|\nabla\times H_z(t)\|_0^2,
\end{aligned}$$

where we used the basic arithmetic–geometric mean inequality. The small parameter $\delta_1 > 0$ is to be determined.

Similarly, we can obtain

$$\begin{aligned}
&\int_0^t\left(\frac{\sigma^*}{2\varepsilon_0\varepsilon_r}\boldsymbol{E}, \nabla\times\frac{\partial H_z}{\partial t}\right)dt = \int_\Omega\int_0^t\frac{\sigma^*}{2\varepsilon_0\varepsilon_r}\boldsymbol{E}\frac{d}{dt}\nabla\times H_z\\
&\quad\le \left(\nabla\times H_z(t), \frac{\sigma^*}{2\varepsilon_0\varepsilon_r}\boldsymbol{E}(t)\right) - \left(\nabla\times H_z(0), \frac{\sigma^*}{2\varepsilon_0\varepsilon_r}\boldsymbol{E}(0)\right) + \frac{C_x}{4\varepsilon_1}\int_0^t\left\|\frac{\partial \boldsymbol{E}}{\partial t}\right\|_0^2 dt + \frac{C_x}{4\varepsilon_1}\int_0^t\|\nabla\times H_z\|_0^2 dt,\\
&\left(\nabla\times H_z(t), \frac{\sigma^*}{2\varepsilon_0\varepsilon_r}\boldsymbol{E}(t)\right) \le \frac{\delta_2C_x^2}{2\varepsilon_1}\varepsilon_0\|\boldsymbol{E}(t)\|_0^2 + \frac{1}{8\delta_2\varepsilon_1\varepsilon_0}\|\nabla\times H_z(t)\|_0^2,\\
&\left(\nabla\times H_z(0), \frac{\sigma^*}{2\varepsilon_0\varepsilon_r}\boldsymbol{E}(0)\right) \le \frac{C_x}{4\varepsilon_1}\|\boldsymbol{E}(0)\|_0^2 + \frac{C_x}{4\varepsilon_1}\|\nabla\times H_z(0)\|_0^2,
\end{aligned}$$

and

$$4\varepsilon_0C_x^2\int_0^t(\nabla\times H_z, \boldsymbol{E})dt \le 2\varepsilon_0C_x^2\int_0^t\|\boldsymbol{E}\|_0^2 + 2\varepsilon_0C_x^2\int_0^t\|\nabla\times H_z\|_0^2.$$

Substituting the above inequalities into (2.33), we have

$$\begin{aligned}
&\frac{\mu_0}{2}\left\|\frac{\partial H_z}{\partial t}(t)\right\|_0^2+\frac{1}{2\mu_0}\left\|\sqrt{\sigma_{mx}^*\sigma_{my}^*}H_z(t)\right\|_0^2+\frac{\varepsilon_0\varepsilon_1}{4}\left\|\frac{\partial \boldsymbol{E}}{\partial t}(t)\right\|_0^2+\frac{1}{4\varepsilon_0\varepsilon_2}\|\nabla\times H_z(t)\|_0^2+4\varepsilon_0\varepsilon_2 C_x^2\|\boldsymbol{E}(t)\|_0^2\\
&\le \mathbf{F}(0)+2\varepsilon_0 C_x^2\int_0^t\|\boldsymbol{E}\|_0^2dt+\left(\frac{C_x}{2}+\frac{C_x}{4\varepsilon_1}\right)\int_0^t\left\|\frac{\partial \boldsymbol{E}}{\partial t}\right\|_0^2dt+\left(\delta_1 C_x^2+\frac{\delta_2}{2\varepsilon_1}C_x^2\right)\varepsilon_0\|\boldsymbol{E}(t)\|_0^2\\
&+\left(\frac{C_x}{2}+\frac{C_x}{4\varepsilon_1}+2\varepsilon_0C_x^2\right)\int_0^t\|\nabla\times H_z\|_0^2+\left(\frac{1}{4\delta_1\varepsilon_0}+\frac{1}{8\varepsilon_0\varepsilon_1\delta_2}\right)\|\nabla\times H_z(t)\|_0^2, \qquad (2.34)
\end{aligned}$$

where $\mathbf{F}(0)=\boldsymbol{g}(0)+(\frac{C_x}{2}+\frac{C_x}{4\varepsilon_1})\|\boldsymbol{E}(0)\|_0^2+(\frac{C_x}{2}+\frac{C_x}{4\varepsilon_1})\|\nabla\times H_z(0)\|_0^2$.

With the choice $\delta_1=2\varepsilon_2$ and $\delta_2=\frac{2\varepsilon_2}{\varepsilon_1}$, we can see that all left hand side terms of (2.34) are larger than the corresponding right hand side terms. Hence by the Gronwall inequality, we conclude the proof. □

3. A fully-discrete finite element scheme and its stability analysis

To design our time-domain finite element method, we first partition Ω by a family of regular meshes $\mathcal{T}_h$ with maximum mesh size h. To accommodate the optical black hole simulation easily, we use a hybrid mesh with mixed types of elements: rectangles in the PML region; triangles elsewhere. For simple implementation, we only use the lowest order Raviart–Thomas–Nédélec's mixed finite element spaces U_h and V_h given as follows: for any rectangular element $e\in\mathcal{T}_h$, we choose

$$\boldsymbol{U}_h=\{\psi_h\in L^2(\Omega):\psi_h|_e\in Q_{0,0},\forall\, e\in\mathcal{T}_h\},$$
$$\boldsymbol{V}_h=\{\boldsymbol{\phi}_h\in H(curl;\Omega):\boldsymbol{\phi}_h|_e\in Q_{0,1}\times Q_{1,0},\forall\, e\in\mathcal{T}_h\},$$

where $Q_{i,j}$ denotes the space of polynomials whose degrees are less than or equal to i and j in variables x and y, respectively. While on a triangular element, we choose

$$\boldsymbol{U}_h=\{\psi_h\in L^2(\Omega):\psi_h|_e \text{ is a constant},\forall\, e\in\mathcal{T}_h\},$$
$$\boldsymbol{V}_h=\{\boldsymbol{\phi}_h\in H(curl;\Omega):\boldsymbol{\phi}_h|_e=span\{\lambda_i\nabla\lambda_j-\lambda_j\nabla\lambda_i\},i,j=1,2,3,\forall\, e\in\mathcal{T}_h\},$$

where λ_i denotes the standard barycentric coordinate at vertex i of element e. To impose the perfect conducting boundary condition $\boldsymbol{n}\times\boldsymbol{E}=\mathbf{0}$, we introduce the space

$$\boldsymbol{V}_h=\{\boldsymbol{\phi}_h\in\boldsymbol{V}_h:\ \boldsymbol{n}\times\boldsymbol{\phi}_h=\mathbf{0}\text{ on }\partial\Omega\}.$$

To define a fully-discrete scheme, we divide the time interval $I=[0,T]$ into N uniform subintervals $I_i=[t_{i-1},t_i]$ by points $t_k=k\tau, k=0,1,...,N$, where $\tau=\frac{T}{N}$. Furthermore, we denote $\boldsymbol{E}^k=\boldsymbol{E}(\cdot\ ,t_k)$, and introduce some difference operators:

$$\delta_\tau\boldsymbol{E}^{k+1}=\frac{\boldsymbol{E}^{k+1}-\boldsymbol{E}^k}{\tau},\qquad \delta_\tau^2\boldsymbol{E}^k=\frac{\boldsymbol{E}^{k+1}-2\boldsymbol{E}^k+\boldsymbol{E}^{k-1}}{\tau^2},$$
$$\delta_{2\tau}\boldsymbol{E}^k=\frac{\boldsymbol{E}^{k+1}-\boldsymbol{E}^{k-1}}{2\tau},\qquad \overline{\boldsymbol{E}}^{k+\frac12}=\frac{\boldsymbol{E}^{k+1}+\boldsymbol{E}^k}{2}.$$

Now we construct a leap-frog type scheme for solving the modeling Eqs. (2.20)–(2.23): for $k=1,2,\ldots$, find $\boldsymbol{E}_h^{k+1}\in\boldsymbol{V}_h^0,\ H_{z,h}^{k+\frac32}\in U_h$ such that

$$\varepsilon_0\left(\varepsilon_r^*\frac{\boldsymbol{E}_h^{k+1}-\boldsymbol{E}_h^k}{\tau},\boldsymbol{\phi}_h\right)+\left(\sigma^*\overline{\boldsymbol{E}}_h^{k+\frac12},\boldsymbol{\phi}_h\right)=\left(H_{z,h}^{k+\frac12},\nabla\times\boldsymbol{\phi}_h\right), \qquad (3.1)$$

$$\mu_0\frac{\boldsymbol{P}_h^{k+\frac32}-\boldsymbol{P}_h^{k+\frac12}}{\tau}=\boldsymbol{E}_h^{k+1}, \qquad (3.2)$$

$$\mu_0 \frac{Q_h^{k+1} - Q_h^k}{\tau} = H_{z,h}^{k+\frac{1}{2}}, \tag{3.3}$$

$$\mu_0 \left(\frac{H_{z,h}^{k+\frac{3}{2}} - H_{z,h}^{k+\frac{1}{2}}}{\tau}, \psi_h \right) + \left((\sigma_{mx}^* + \sigma_{my}^*) \overline{H}_{z,h}^{k+1}, \psi_h \right) + \left(\nabla \times \boldsymbol{E}_h^{k+1}, \psi_h \right)$$
$$+ (\sigma_{mx}^* \sigma_{my}^* Q_h^{k+1}, \psi_h) + \mu_0 \left(\nabla \times \overline{\boldsymbol{P}}_h^{*,k+1}, \psi_h \right) = 0, \tag{3.4}$$

hold true for any $\boldsymbol{\phi}_h \in \boldsymbol{V}_h^0$ and any $\psi_h \in U_h$, where $\boldsymbol{P}^* = (k_1 P_x, k_2 P_y)'$.

In the rest of this section, we carry out the stability analysis for our scheme (3.1)–(3.4).

Theorem 3.1. *Denote the wave speed in free space by $C_v = \frac{1}{\sqrt{\varepsilon_0 \mu_0}}$, and $C_{inv} > 0$ for the constant in the standard inverse inequality:*

$$\|\nabla \times \boldsymbol{v}_h\|_0 \le C_{inv} h^{-1} \|\boldsymbol{v}_h\|_0, \quad \forall\, \boldsymbol{v}_h \in \boldsymbol{V}_h. \tag{3.5}$$

If the time step τ satisfies the constraint

$$\tau \le \min \left\{ \frac{h}{3C_{inv}C_v}, \frac{h}{3C_{inv}C_x}, \frac{1}{5\mu_0\varepsilon_1 C_x^2}, \frac{1}{4C_v}, \frac{1}{12\varepsilon_2 C_x}, \frac{2\varepsilon_1 C_v}{35\varepsilon_2^2 C_x^2}, \frac{7h\varepsilon_2^2 C_x}{3\varepsilon_1 C_{inv} C_v^2} \right\}, \tag{3.6}$$

then for any $n \ge 1$ we have

$$\varepsilon_0 \|\delta_\tau \boldsymbol{E}_h^n\|_0^2 + \varepsilon_0 \|\boldsymbol{E}_h^n\|_0^2 + \mu_0 \|\delta_\tau H_{z,h}^{n+\frac{1}{2}}\|_0^2 + \mu_0 \|H_{z,h}^{n+\frac{1}{2}}\|_0^2$$
$$+ \mu_0 \|\boldsymbol{P}_h^{n+\frac{1}{2}}\|_0^2 + \mu_0 \|\delta_\tau \boldsymbol{P}_h^{n+\frac{1}{2}}\|_0^2 + \mu_0 \|Q_h^n\|_0^2 + \mu_0 \|\delta_\tau Q_h^n\|_0^2 \le C F_h(0),$$

where $C > 0$ is a constant, and the function $F_h(0)$ depends on initial conditions $\boldsymbol{E}_h^0$, $\delta_\tau \boldsymbol{E}_h^0$, $H_{z,h}^{\frac{1}{2}}$, $\delta_\tau H_{z,h}^{\frac{1}{2}}$, $\boldsymbol{P}_h^{\frac{1}{2}}$, $\delta_\tau \boldsymbol{P}_h^{\frac{1}{2}}$, Q_h^0, $\delta_\tau Q_h^0$, $\nabla \times \boldsymbol{E}_h^0$, $\nabla \times \boldsymbol{E}_h^{-1}$, $\nabla \times \delta_\tau \boldsymbol{E}_h^0$, $\nabla \times \boldsymbol{P}_h^{\frac{1}{2}}$, and $\nabla \times \delta_\tau \boldsymbol{P}_h^{-\frac{1}{2}}$.

Proof. Subtracting Eqs. (3.1) and (3.4) from themselves with k reduced by 1, respectively, then dividing the resultants by τ, we have

$$\varepsilon_0 \left(\varepsilon_r^* \frac{\delta_\tau \boldsymbol{E}_h^{k+1} - \delta_\tau \boldsymbol{E}_h^k}{\tau}, \boldsymbol{\phi}_h \right) + \left(\sigma^* \delta_{2\tau} \boldsymbol{E}_h^k, \boldsymbol{\phi}_h \right) = \left(\delta_\tau H_{z,h}^{k+\frac{1}{2}}, \nabla \times \boldsymbol{\phi}_h \right), \tag{3.7}$$

$$\mu_0 \left(\delta_\tau^2 H_{z,h}^{k+\frac{1}{2}}, \psi_h \right) + \left((\sigma_{mx}^* + \sigma_{my}^*) \delta_{2\tau} H_{z,h}^{k+\frac{1}{2}}, \psi_h \right) + \left(\nabla \times \delta_\tau \boldsymbol{E}_h^{k+1}, \psi_h \right)$$
$$+ (\sigma_{mx}^* \sigma_{my}^* \delta_\tau Q_h^{k+1}, \psi_h) + \mu_0 \left(\nabla \times \delta_\tau \overline{\boldsymbol{P}}_h^{*,k+1}, \psi_h \right) = 0. \tag{3.8}$$

Choosing $\phi_h = 2\tau\delta_{2\tau}\boldsymbol{E}_h^k = \boldsymbol{E}_h^{k+1} - \boldsymbol{E}_h^{k-1} = \tau(\delta_\tau \boldsymbol{E}_h^{k+1} + \delta_\tau \boldsymbol{E}_h^k)$ and $\psi_h = 2\tau\delta_{2\tau} H_{z,h}^{k+\frac{1}{2}}$ in (3.7) and (3.8), respectively, we have

$$\varepsilon_0 \left(\|\sqrt{\varepsilon_r^*}\delta_\tau \boldsymbol{E}_h^{k+1}\|_0^2 - \|\sqrt{\varepsilon_r^*}\delta_\tau \boldsymbol{E}_h^k\|_0^2 \right) \le 2\tau \left(\delta_\tau H_{z,h}^{k+\frac{1}{2}}, \nabla \times \delta_{2\tau} \boldsymbol{E}_h^k \right), \tag{3.9}$$

$$\mu_0 \left(\|\delta_\tau H_{z,h}^{k+\frac{3}{2}}\|_0^2 - \|\delta_\tau H_{z,h}^{k+\frac{1}{2}}\|_0^2 \right) \le -2\tau \left(\nabla \times \delta_\tau \boldsymbol{E}_h^{k+1}, \delta_{2\tau} H_{z,h}^{k+\frac{1}{2}} \right)$$
$$- 2\tau \left(\sigma_{mx}^* \sigma_{my}^* \delta_\tau Q_h^{k+1}, \delta_{2\tau} H_{z,h}^{k+\frac{1}{2}} \right) - 2\tau\mu_0 \left(\nabla \times \delta_\tau \overline{\boldsymbol{P}}_h^{*,k+1}, \delta_{2\tau} H_{z,h}^{k+\frac{1}{2}} \right). \tag{3.10}$$

Choosing $\phi_h = \tau(E_h^{k+1} + E_h^k)$ and $\psi_h = \tau(H_{z,h}^{k+\frac{3}{2}} + H_{z,h}^{k+\frac{1}{2}})$ in (3.1) and (3.4), respectively, we obtain

$$\varepsilon_0 \left(\|\sqrt{\varepsilon_r^*}\boldsymbol{E}_h^{k+1}\|_0^2 - \|\sqrt{\varepsilon_r^*}\boldsymbol{E}_h^k\|_0^2 \right) \le \tau \left(H_{z,h}^{k+\frac{1}{2}}, \nabla \times (\boldsymbol{E}_h^{k+1} + \boldsymbol{E}_h^k) \right), \tag{3.11}$$

$$\begin{aligned} \mu_0 \left(\|H_{z,h}^{k+\frac{3}{2}}\|_0^2 - \|H_{z,h}^{k+\frac{1}{2}}\|_0^2 \right) &\le -\tau \left(\nabla \times \boldsymbol{E}_h^{k+1}, H_{z,h}^{k+\frac{3}{2}} + H_{z,h}^{k+\frac{1}{2}} \right) \\ &\quad - \tau \left(\sigma_{mx}^* \sigma_{my}^* Q_h^{k+1}, H_{z,h}^{k+\frac{3}{2}} + H_{z,h}^{k+\frac{1}{2}} \right) - \tau\mu_0 \left(\nabla \times \overline{\boldsymbol{P}}_h^{*,k+1}, H_{z,h}^{k+\frac{3}{2}} + H_{z,h}^{k+\frac{1}{2}} \right). \end{aligned} \tag{3.12}$$

Denote the constant $C_k = 7\frac{\varepsilon_2^2 C_x^2}{\varepsilon_1 C_v^2}$. From Eqs. (3.2)–(3.3), we easily obtain

$$\mu_0 \left(\|\boldsymbol{P}_h^{k+\frac{3}{2}}\|_0^2 - \|\boldsymbol{P}_h^{k+\frac{1}{2}}\|_0^2 \right) = \tau \left(\boldsymbol{E}_h^{k+1}, \boldsymbol{P}_h^{k+\frac{3}{2}} + \boldsymbol{P}_h^{k+\frac{1}{2}} \right), \tag{3.13}$$

$$\mu_0 C_k \left(\|\delta_\tau \boldsymbol{P}_h^{k+\frac{3}{2}}\|_0^2 - \|\delta_\tau \boldsymbol{P}_h^{k+\frac{1}{2}}\|_0^2 \right) = \tau C_k \left(\delta_\tau \boldsymbol{E}_h^{k+1}, \delta_\tau \boldsymbol{P}_h^{k+\frac{3}{2}} + \delta_\tau \boldsymbol{P}_h^{k+\frac{1}{2}} \right), \tag{3.14}$$

$$\mu_0 \left(\|Q_h^{k+1}\|_0^2 - \|Q_h^k\|_0^2 \right) = \tau \left(H_{z,h}^{k+\frac{1}{2}}, Q_h^{k+1} + Q_h^k \right), \tag{3.15}$$

$$\mu_0 \left(\|\delta_\tau Q_h^{k+1}\|_0^2 - \|\delta_\tau Q_h^k\|_0^2 \right) = \tau \left(\delta_\tau H_{z,h}^{k+\frac{1}{2}}, \delta_\tau Q_h^{k+1} + \delta_\tau Q_h^k \right). \tag{3.16}$$

Adding up (3.9)–(3.16), and summing up the result for k from 0 to $n-1$, we obtain

$$\begin{aligned} &\varepsilon_0 \left(\|\sqrt{\varepsilon_r^*}\delta_\tau \boldsymbol{E}_h^n\|_0^2 - \|\sqrt{\varepsilon_r^*}\delta_\tau \boldsymbol{E}_h^0\|_0^2 \right) + \varepsilon_0 \left(\|\sqrt{\varepsilon_r^*}\boldsymbol{E}_h^n\|_0^2 - \|\sqrt{\varepsilon_r^*}\boldsymbol{E}_h^0\|_0^2 \right) \\ &\quad + \mu_0 \left(\|\delta_\tau H_{z,h}^{n+\frac{1}{2}}\|_0^2 - \|\delta_\tau H_{z,h}^{\frac{1}{2}}\|_0^2 \right) + \mu_0 \left(\|H_{z,h}^{n+\frac{1}{2}}\|_0^2 - \|H_{z,h}^{\frac{1}{2}}\|_0^2 \right) \\ &\quad + \mu_0 \left(\|\boldsymbol{P}_h^{n+\frac{1}{2}}\|_0^2 - \|\boldsymbol{P}_h^{\frac{1}{2}}\|_0^2 \right) + \mu_0 C_k \left(\|\delta_\tau \boldsymbol{P}_h^{n+\frac{1}{2}}\|_0^2 - \|\delta_\tau \boldsymbol{P}_h^{\frac{1}{2}}\|_0^2 \right) \\ &\quad + \mu_0 \left(\|Q_h^n\|_0^2 - \|Q_h^0\|_0^2 \right) + \mu_0 \left(\|\delta_\tau Q_h^n\|_0^2 - \|\delta_\tau Q_h^0\|_0^2 \right) \\ &\le \sum_{k=0}^{n-1} 2\tau \left[\left(\delta_\tau H_{z,h}^{k+\frac{1}{2}}, \nabla \times \delta_{2\tau} \boldsymbol{E}_h^k \right) - \left(\nabla \times \delta_\tau \boldsymbol{E}_h^{k+1}, \delta_{2\tau} H_{z,h}^{k+\frac{1}{2}} \right) \right] \\ &\quad - \sum_{k=0}^{n-1} 2\tau \left(\sigma_{mx}^* \sigma_{my}^* \delta_\tau Q_h^{k+1}, \delta_{2\tau} H_{z,h}^{k+\frac{1}{2}} \right) - \sum_{k=0}^{n-1} 2\tau\mu_0 \left(\nabla \times \delta_\tau \overline{\boldsymbol{P}}_h^{*,k+1}, \delta_{2\tau} H_{z,h}^{k+\frac{1}{2}} \right) \\ &\quad + \sum_{k=0}^{n-1} \tau \left[\left(H_{z,h}^{k+\frac{1}{2}}, \nabla \times (\boldsymbol{E}_h^{k+1} + \boldsymbol{E}_h^k) \right) - \left(\nabla \times \boldsymbol{E}_h^{k+1}, H_{z,h}^{k+\frac{3}{2}} + H_{z,h}^{k+\frac{1}{2}} \right) \right] \\ &\quad - \sum_{k=0}^{n-1} \tau \left(\sigma_{mx}^* \sigma_{my}^* Q_h^{k+1}, H_{z,h}^{k+\frac{3}{2}} + H_{z,h}^{k+\frac{1}{2}} \right) - \sum_{k=0}^{n-1} \tau\mu_0 \left(\nabla \times \overline{\boldsymbol{P}}_h^{*,k+1}, H_{z,h}^{k+\frac{3}{2}} + H_{z,h}^{k+\frac{1}{2}} \right) \\ &\quad + \sum_{k=0}^{n-1} \tau \left(\boldsymbol{E}_h^{k+1}, \boldsymbol{P}_h^{k+\frac{3}{2}} + \boldsymbol{P}_h^{k+\frac{1}{2}} \right) + \sum_{k=0}^{n-1} \tau \left(H_{z,h}^{k+\frac{1}{2}}, Q_h^{k+1} + Q_h^k \right) \\ &\quad + \sum_{k=0}^{n-1} \tau C_k \left(\delta_\tau \boldsymbol{E}_h^{k+1}, \delta_\tau \boldsymbol{P}_h^{k+\frac{3}{2}} + \delta_\tau \boldsymbol{P}_h^{k+\frac{1}{2}} \right) + \sum_{k=0}^{n-1} \tau \left(\delta_\tau H_{z,h}^{k+\frac{1}{2}}, \delta_\tau Q_h^{k+1} + \delta_\tau Q_h^k \right) \\ &= \sum_{i=1}^{10} Err_i. \end{aligned} \tag{3.17}$$

Below we will estimate all Err_i terms. First, note that

$$
\begin{aligned}
Err_1 &= \sum_{k=0}^{n-1} 2\tau \left[\left(\delta_\tau H_{z,h}^{k+\frac{1}{2}}, \nabla \times \delta_{2\tau} \boldsymbol{E}_h^k \right) - \left(\nabla \times \delta_\tau \boldsymbol{E}_h^{k+1}, \delta_{2\tau} H_{z,h}^{k+\frac{1}{2}} \right) \right] \\
&= \tau \sum_{k=0}^{n-1} \left[\left(\delta_\tau H_{z,h}^{k+\frac{1}{2}}, \nabla \times \delta_\tau \boldsymbol{E}_h^k \right) - \left(\delta_\tau H_{z,h}^{k+\frac{3}{2}}, \nabla \times \delta_\tau \boldsymbol{E}_h^{k+1} \right) \right] \\
&= \tau \left(\delta_\tau H_{z,h}^{\frac{1}{2}}, \nabla \times \delta_\tau \boldsymbol{E}_h^0 \right) - \tau \left(\delta_\tau H_{z,h}^{n+\frac{1}{2}}, \nabla \times \delta_\tau \boldsymbol{E}_h^n \right).
\end{aligned} \tag{3.18}
$$

Using the Cauchy–Schwarz inequality and the inverse inequality (3.5), we obtain

$$
\begin{aligned}
\tau \left(\delta_\tau H_{z,h}^{n+\frac{1}{2}}, \nabla \times \delta_\tau \boldsymbol{E}_h^n \right) &\leq \tau C_{inv} h^{-1} C_v \cdot \sqrt{\varepsilon_0} \|\delta_\tau \boldsymbol{E}_h^n\|_0 \cdot \sqrt{\mu_0} \|\delta_\tau H_{z,h}^{n+\frac{1}{2}}\|_0 \\
&\leq \frac{\tau C_{inv} h^{-1} C_v}{2} \left(\varepsilon_0 \|\delta_\tau \boldsymbol{E}_h^n\|_0^2 + \mu_0 \|\delta_\tau H_{z,h}^{n+\frac{1}{2}}\|_0^2 \right),
\end{aligned}
$$

from which and (3.18), we have

$$
Err_1 \leq \frac{\tau C_v}{2} \left(\mu_0 \|\delta_\tau H_{z,h}^{\frac{1}{2}}\|_0^2 + \varepsilon_0 \|\nabla \times \delta_\tau \boldsymbol{E}_h^0\|_0^2 \right) + \frac{\tau C_{inv} h^{-1} C_v}{2} \left(\varepsilon_0 \|\delta_\tau \boldsymbol{E}_h^n\|_0^2 + \mu_0 \|\delta_\tau H_{z,h}^{n+\frac{1}{2}}\|_0^2 \right).
$$

Using the Cauchy–Schwarz inequality and the definition of C_x, we easily have

$$
\begin{aligned}
Err_2 &= -\sum_{k=0}^{n-1} 2\tau \left(\sigma_{mx}^* \sigma_{my}^* \delta_\tau Q_h^{k+1}, \delta_{2\tau} H_{z,h}^{k+\frac{1}{2}} \right) = -\tau \sum_{k=0}^{n-1} \left(\sigma_{mx}^* \sigma_{my}^* \delta_\tau Q_h^{k+1}, \delta_\tau H_{z,h}^{k+\frac{3}{2}} + \delta_\tau H_{z,h}^{k+\frac{1}{2}} \right) \\
&\leq \frac{\tau \mu_0 C_x^2}{2} \sum_{k=0}^{n-1} \mu_0 \|\delta_\tau Q_h^{k+1}\|_0^2 + \tau \mu_0 C_x^2 \cdot \mu_0 \|\delta_\tau H_{z,h}^{n+\frac{1}{2}}\|_0^2 + 2\tau \mu_0 C_x^2 \sum_{k=0}^{n-1} \mu_0 \|\delta_\tau H_{z,h}^{k+\frac{1}{2}}\|_0^2.
\end{aligned}
$$

Similar to Err_1, we have

$$
\begin{aligned}
Err_4 &= \sum_{k=0}^{n-1} \tau \left[\left(H_{z,h}^{k+\frac{1}{2}}, \nabla \times (\boldsymbol{E}_h^{k+1} + \boldsymbol{E}_h^k) \right) - \left(\nabla \times \boldsymbol{E}_h^{k+1}, H_{z,h}^{k+\frac{3}{2}} + H_{z,h}^{k+\frac{1}{2}} \right) \right] \\
&= \tau \sum_{k=0}^{n-1} \left[\left(H_{z,h}^{k+\frac{1}{2}}, \nabla \times \boldsymbol{E}_h^k \right) - \left(H_{z,h}^{k+\frac{3}{2}}, \nabla \times \boldsymbol{E}_h^{k+1} \right) \right] \\
&= \tau \left(H_{z,h}^{\frac{1}{2}}, \nabla \times \boldsymbol{E}_h^0 \right) - \tau \left(H_{z,h}^{n+\frac{1}{2}}, \nabla \times \boldsymbol{E}_h^n \right) \\
&\leq \frac{\tau C_v}{2} \left(\mu_0 \|H_{z,h}^{\frac{1}{2}}\|_0^2 + \varepsilon_0 \|\nabla \times \boldsymbol{E}_h^0\|_0^2 \right) + \frac{\tau C_{inv} h^{-1} C_v}{2} \left(\varepsilon_0 \|\boldsymbol{E}_h^n\|_0^2 + \mu_0 \|H_{z,h}^{n+\frac{1}{2}}\|_0^2 \right).
\end{aligned}
$$

Similar to Err_2, we can obtain

$$
\begin{aligned}
Err_5 &= -\sum_{k=0}^{n-1} \tau \left(\sigma_{mx}^* \sigma_{my}^* Q_h^{k+1}, H_{z,h}^{k+\frac{3}{2}} + H_{z,h}^{k+\frac{1}{2}} \right) \\
&\leq \frac{\tau \mu_0 C_x^2}{2} \sum_{k=0}^{n-1} \mu_0 \|Q_{z,h}^{k+1}\|_0^2 + \tau \mu_0 C_x^2 \cdot \mu_0 \|H_{z,h}^{n+\frac{1}{2}}\|_0^2 + 2\tau \mu_0 C_x^2 \sum_{k=0}^{n-1} \mu_0 \|H_{z,h}^{k+\frac{1}{2}}\|_0^2.
\end{aligned}
$$

Using the Cauchy–Schwarz inequality, we easily have

$$
\begin{aligned}
Err_7 &= \tau \sum_{k=0}^{n-1} \left(\boldsymbol{E}_h^{k+1}, \boldsymbol{P}_h^{k+\frac{3}{2}} + \boldsymbol{P}_h^{k+\frac{1}{2}} \right) \\
&\le \frac{\tau C_v}{2} \sum_{k=0}^{n-1} \varepsilon_0 \|\boldsymbol{E}_h^{k+1}\|_0^2 + 2\tau C_v \sum_{k=0}^{n-1} \mu_0 \|\boldsymbol{P}_h^{k+\frac{1}{2}}\|_0^2 + \tau C_v \left(\mu_0 \|\boldsymbol{P}_h^{n+\frac{1}{2}}\|_0^2 \right),
\end{aligned}
$$

and

$$
\begin{aligned}
Err_8 &= \tau \sum_{k=0}^{n-1} \left(H_{z,h}^{k+\frac{1}{2}}, Q_h^{k+1} + Q_h^k \right) \\
&\le \frac{\tau}{2\mu_0} \sum_{k=0}^{n-1} \mu_0 \| H_{z,h}^{k+\frac{3}{2}} \|_0^2 + \frac{2\tau}{\mu_0} \sum_{k=0}^{n-1} \mu_0 \| Q_h^k \|_0^2 + \frac{\tau}{\mu_0} \cdot \mu_0 \| Q_h^n \|_0^2.
\end{aligned}
$$

Similar to Err_2, we can obtain

$$
\begin{aligned}
Err_9 &= \tau \sum_{k=0}^{n-1} C_k \left(\delta_\tau \boldsymbol{E}_h^{k+1}, \delta_\tau \boldsymbol{P}_h^{k+\frac{3}{2}} + \delta_\tau \boldsymbol{P}_h^{k+\frac{1}{2}} \right) \\
&\le \frac{\tau C_v C_k}{2} \sum_{k=0}^{n-1} \varepsilon_0 \|\boldsymbol{E}_h^{k+1}\|_0^2 + \tau C_v C_k \mu_0 \|\delta_\tau \boldsymbol{P}_{z,h}^{n+\frac{1}{2}}\|_0^2 + 2\tau C_v C_k \sum_{k=0}^{n-1} \mu_0 \|\delta_\tau \boldsymbol{P}_{z,h}^{k+\frac{1}{2}}\|_0^2,
\end{aligned}
$$

and

$$
\begin{aligned}
Err_{10} &= \sum_{k=0}^{n-1} \tau \left(\delta_\tau H_{z,h}^{k+\frac{1}{2}}, \delta_\tau Q_h^{k+1} + \delta_\tau Q_h^k \right) \\
&\le \frac{\tau}{2\mu_0} \sum_{k=0}^{n-1} \mu_0 \|\delta_\tau H_{z,h}^{k+\frac{1}{2}}\|_0^2 + \tau \|\delta_\tau Q_h^n\|_0^2 + \frac{2\tau}{\mu_0} \sum_{k=0}^{n-1} \mu_0 \|\delta_\tau Q_h^k\|_0^2.
\end{aligned}
$$

Now we just need to estimate the last two difficult terms Err_3 and Err_6. Let us consider Err_3 first. Adding up Err_3 and (3.7) with $\phi_h = \tau\mu_0 \delta_\tau (\frac{\boldsymbol{P}_h^{*,k+\frac{3}{2}} + \boldsymbol{P}_h^{*,k-\frac{1}{2}}}{2} + \boldsymbol{P}_h^{*,k+\frac{1}{2}})$, we have

$$
\begin{aligned}
Err_3 &= -\sum_{k=0}^{n-1} 2\tau\mu_0 \left(\nabla \times \delta_\tau \overline{\boldsymbol{P}}_h^{*,k+1}, \delta_{2\tau} H_{z,h}^{k+\frac{1}{2}} \right) \\
&= \left[-\sum_{k=0}^{n-1} 2\tau\mu_0 \left(\nabla \times \delta_\tau \left(\frac{\boldsymbol{P}_h^{*,k+\frac{3}{2}} + \boldsymbol{P}_h^{*,k+\frac{1}{2}}}{2} \right), \delta_{2\tau} H_{z,h}^{k+\frac{1}{2}} \right) \right. \\
&\quad \left. + \sum_{k=0}^{n-1} \tau\mu_0 \left(\delta_\tau H_{z,h}^{k+\frac{1}{2}}, \nabla \times \delta_\tau \left(\frac{\boldsymbol{P}_h^{*,k+\frac{3}{2}} + \boldsymbol{P}_h^{*,k-\frac{1}{2}}}{2} + \boldsymbol{P}_h^{*,k+\frac{1}{2}} \right) \right) \right] \\
&\quad - \sum_{k=0}^{n-1} \tau\mu_0 \left(\varepsilon_0 \varepsilon_r^* \delta_\tau^2 \boldsymbol{E}_h^k, \delta_\tau \left(\frac{\boldsymbol{P}_h^{*,k+\frac{3}{2}} + \boldsymbol{P}_h^{*,k-\frac{1}{2}}}{2} + \boldsymbol{P}_h^{*,k+\frac{1}{2}} \right) \right) \\
&\quad - \sum_{k=0}^{n-1} \tau\mu_0 \left(\sigma^* \delta_{2\tau} \boldsymbol{E}_h^k, \delta_\tau \left(\frac{\boldsymbol{P}_h^{*,k+\frac{3}{2}} + \boldsymbol{P}_h^{*,k-\frac{1}{2}}}{2} + \boldsymbol{P}_h^{*,k+\frac{1}{2}} \right) \right) = \sum_{i=1}^{3} rhs_i. \qquad (3.19)
\end{aligned}
$$

Using the fact that $\boldsymbol{P}_h^{n-\frac{1}{2}} = \boldsymbol{P}_h^{n+\frac{1}{2}} - \tau\delta_\tau \boldsymbol{P}_h^{n+\frac{1}{2}} = \boldsymbol{P}_h^{n+\frac{1}{2}} - \frac{\tau}{\mu_0}\boldsymbol{E}_h^n$ and the estimate

$$\|\boldsymbol{P}_h^{*,k}\|_0 = \| \begin{bmatrix} k_1 & 0 \\ 0 & k_2 \end{bmatrix} \boldsymbol{P}_h^k\|_0 \le C_x \|\boldsymbol{P}_h^k\|_0,$$

we obtain

$$\begin{aligned}
-\tau\mu_0 \left(\nabla \times \delta_\tau \frac{\boldsymbol{P}_h^{*,n+\frac{1}{2}} + \boldsymbol{P}_h^{*,n-\frac{1}{2}}}{2}, \delta_\tau H_{z,h}^{n+\frac{1}{2}} \right) &\le \frac{\tau\mu_0 C_{inv} h^{-1} C_x}{2} \left(\left\| \delta_\tau \frac{\boldsymbol{P}_h^{n+\frac{1}{2}} + \boldsymbol{P}_h^{n-\frac{1}{2}}}{2} \right\|_0^2 + \|\delta_\tau H_{z,h}^{n+\frac{1}{2}}\|_0^2 \right) \\
&\le \frac{\tau\mu_0 C_{inv} h^{-1} C_x}{2} \left(\frac{1}{2}\|\delta_\tau \boldsymbol{P}_h^{n+\frac{1}{2}}\|_0^2 + \frac{1}{2}\|\delta_\tau \boldsymbol{P}_h^{n-\frac{1}{2}}\|_0^2 + \|\delta_\tau H_{z,h}^{n+\frac{1}{2}}\|_0^2 \right) \\
&= \frac{\tau\mu_0 C_{inv} h^{-1} C_x}{4}\|\delta_\tau \boldsymbol{P}_h^{n+\frac{1}{2}}\|_0^2 + \frac{\tau\mu_0 C_{inv} h^{-1} C_x}{4}\|\delta_\tau \boldsymbol{P}_h^{n+\frac{1}{2}} - \frac{\tau}{\mu_0}\delta_\tau \boldsymbol{E}_h^n\|_0^2 + \frac{\tau\mu_0 C_{inv} h^{-1} C_x}{2}\|\delta_\tau H_{z,h}^{n+\frac{1}{2}}\|_0^2 \\
&\le \frac{3\tau\mu_0 C_{inv} h^{-1} C_x}{4}\|\delta_\tau \boldsymbol{P}_h^{n+\frac{1}{2}}\|_0^2 + \frac{\tau^3 C_{inv} h^{-1} C_x}{2\mu_0}\|\delta_\tau \boldsymbol{E}_h^n\|_0^2 + \frac{\tau\mu_0 C_{inv} h^{-1} C_x}{2}\|\delta_\tau H_{z,h}^{n+\frac{1}{2}}\|_0^2 \\
&= \frac{3\tau\mu_0 C_{inv} h^{-1} C_x}{4}\|\delta_\tau \boldsymbol{P}_h^{n+\frac{1}{2}}\|_0^2 + \frac{\tau^3 C_{inv} h^{-1} C_x C_v^2}{2}\varepsilon_0\|\delta_\tau \boldsymbol{E}_h^n\|_0^2 + \frac{\tau\mu_0 C_{inv} h^{-1} C_x}{2}\|\delta_\tau H_{z,h}^{n+\frac{1}{2}}\|_0^2,
\end{aligned}$$

substituting which into rhs_1, we have

$$\begin{aligned}
rhs_1 &= -\sum_{k=0}^{n-1} 2\tau\mu_0 \left(\nabla \times \delta_\tau \left(\frac{\boldsymbol{P}_h^{*,k+\frac{3}{2}} + \boldsymbol{P}_h^{*,k+\frac{1}{2}}}{2} \right), \delta_{2\tau} H_{z,h}^{k+\frac{1}{2}} \right) \\
&\quad + \sum_{k=0}^{n-1} \tau\mu_0 \left(\delta_\tau H_{z,h}^{k+\frac{1}{2}}, \nabla \times \delta_\tau \left(\frac{\boldsymbol{P}_h^{*,k+\frac{3}{2}} + \boldsymbol{P}_h^{*,k-\frac{1}{2}}}{2} + \boldsymbol{P}_h^{*,k+\frac{1}{2}} \right) \right) \\
&= \tau\mu_0 \sum_{k=0}^{n-1} \left[\left(\nabla \times \delta_\tau \frac{\boldsymbol{P}_h^{*,k+\frac{1}{2}} + \boldsymbol{P}_h^{*,k-\frac{1}{2}}}{2}, \delta_\tau H_{z,h}^{k+\frac{1}{2}} \right) - \left(\nabla \times \delta\tau \frac{\boldsymbol{P}_h^{*,k+\frac{3}{2}} + \boldsymbol{P}_h^{*,k+\frac{1}{2}}}{2}, \delta_\tau H_{z,h}^{k+\frac{3}{2}} \right) \right] \\
&= \tau\mu_0 \left(\nabla \times \delta_\tau \frac{\boldsymbol{P}_h^{*,\frac{1}{2}} + \boldsymbol{P}_h^{*,-\frac{1}{2}}}{2}, \delta_\tau H_{z,h}^{\frac{1}{2}} \right) - \tau\mu_0 \left(\nabla \times \delta_\tau \frac{\boldsymbol{P}_h^{*,n+\frac{1}{2}} + \boldsymbol{P}_h^{*,n-\frac{1}{2}}}{2}, \delta_\tau H_{z,h}^{n+\frac{1}{2}} \right) \\
&\le \frac{\tau}{4}\left(\|\nabla \times \boldsymbol{E}_h^{*,0}\|_0^2 + \|\nabla \times \boldsymbol{E}_h^{*,-1}\|_0^2 \right) + \frac{\tau}{2}\|\delta_\tau H_{z,h}^{\frac{1}{2}}\|_0^2 + \frac{3\tau C_{inv} h^{-1} C_x}{4}\mu_0\|\delta_\tau \boldsymbol{P}_h^{n+\frac{1}{2}}\|_0^2 \\
&\quad + \frac{\tau^3 C_{inv} h^{-1} C_x C_v^2}{2}\varepsilon_0\|\delta\tau \boldsymbol{E}_h^n\|_0^2 + \frac{\tau C_{inv} h^{-1} C_x}{2}\mu_0\|\delta_\tau H_{z,h}^{n+\frac{1}{2}}\|_0^2,
\end{aligned} \tag{3.20}$$

Using (3.2), we have

$$\begin{aligned}
rhs_2 &= -\sum_{k=0}^{n-1} \tau\mu_0 \left(\varepsilon_0 \varepsilon_r^* \delta_\tau^2 \boldsymbol{E}_h^k, \delta_\tau \left(\frac{\boldsymbol{P}_h^{*,k+\frac{3}{2}} + \boldsymbol{P}_h^{*,k-\frac{1}{2}}}{2} + \boldsymbol{P}_h^{*,k+\frac{1}{2}} \right) \right) \\
&= -\tau \sum_{k=0}^{n-1} \varepsilon_0 \left(\varepsilon_r^* \frac{\boldsymbol{E}_h^{k+1} - 2\boldsymbol{E}_h^k + \boldsymbol{E}_h^{k-1}}{\tau^2}, \frac{\boldsymbol{E}_h^{*,k+1} - 2\boldsymbol{E}_h^{*,k} + \boldsymbol{E}_h^{*,k-1}}{2} + 2\boldsymbol{E}_h^{*,k} \right)
\end{aligned}$$

$$\leq -\tau\varepsilon_0 \sum_{k=0}^{n-1} \left(\varepsilon_r^* \frac{\boldsymbol{E}_h^{k+1} - 2\boldsymbol{E}_h^k + \boldsymbol{E}_h^{k-1}}{\tau^2}, 2\boldsymbol{E}_h^{*,k} \right) = -2\varepsilon_0 \sum_{k=0}^{n-1} \left(\varepsilon_r^* \delta_\tau \boldsymbol{E}_h^{k+1} - \varepsilon_r^* \delta_\tau \boldsymbol{E}_h^k, \boldsymbol{E}_h^{*,k} \right)$$

$$= -2\varepsilon_0 \left(\varepsilon_r^* \delta_\tau \boldsymbol{E}_h^n, \boldsymbol{E}_h^{*,n-1} \right) + 2\varepsilon_0 \left(\varepsilon_r^* \delta_\tau \boldsymbol{E}_h^0, \boldsymbol{E}_h^{*,0} \right) + 2\varepsilon_0 \sum_{k=1}^{n-1} \left(\varepsilon_r^* \delta_\tau \boldsymbol{E}_h^k, \boldsymbol{E}_h^{*,k} - \boldsymbol{E}_h^{*,k-1} \right). \tag{3.21}$$

By the arithmetic–geometric mean inequality, we have

$$\begin{aligned} -2\varepsilon_0 \left(\varepsilon_r^* \delta_\tau \boldsymbol{E}_h^n, \boldsymbol{E}_h^{*,n-1} \right) &= 2\varepsilon_0 \left(\varepsilon_r^* \delta_\tau \boldsymbol{E}_h^n, \tau\delta_\tau \boldsymbol{E}_h^{*,n} - \boldsymbol{E}_h^{*,n} \right) \\ &= 2\varepsilon_0 \left(\varepsilon_r^* \delta_\tau \boldsymbol{E}_h^n, \tau\delta_\tau \boldsymbol{E}_h^{*,n} \right) - 2\varepsilon_0 \left(\varepsilon_r^* \delta_\tau \boldsymbol{E}_h^n, \mu_0 \delta_\tau \boldsymbol{P}_h^{*,n+\frac{1}{2}} \right) \\ &\leq 2\tau C_x \varepsilon_2 \varepsilon_0 \|\delta_\tau \boldsymbol{E}_h^n\|_0^2 + \delta_1 \varepsilon_2 \varepsilon_0 \|\delta_\tau \boldsymbol{E}_h^n\|_0^2 + \frac{\varepsilon_2 C_x^2}{\delta_1 C_v^2} \mu_0 \|\delta_\tau \boldsymbol{P}_h^{n+\frac{1}{2}}\|_0^2, \end{aligned}$$

where $\delta_1 > 0$ is a small constant to be determined. Hence we have

$$\begin{aligned} rhs_2 \leq\ & 2\tau C_x \varepsilon_2 \varepsilon_0 \|\delta_\tau \boldsymbol{E}_h^n\|_0^2 + \delta_1 \varepsilon_2 \varepsilon_0 \|\delta_\tau \boldsymbol{E}_h^n\|_0^2 + \frac{C_x^2 \varepsilon_2}{C_v^2 \delta_1} \mu_0 \|\delta_\tau \boldsymbol{P}_h^{n+\frac{1}{2}}\|_0^2 \\ & + \varepsilon_0 \varepsilon_2 C_x \|\boldsymbol{E}_h^0\|_0^2 + \varepsilon_0 \varepsilon_2 C_x \|\delta_\tau \boldsymbol{E}_h^0\|_0^2 + \tau \varepsilon_0 \varepsilon_2 C_x \sum_{k=1}^{n-1} \|\delta_\tau \boldsymbol{E}_h^k\|_0^2. \end{aligned}$$

Similarly, we can obtain

$$\begin{aligned} rhs_3 &= -\sum_{k=0}^{n-1} \tau\mu_0 \left(\sigma^* \delta_{2\tau} \boldsymbol{E}_h^k, \delta_\tau \frac{\boldsymbol{P}_h^{*,k+\frac{3}{2}} + \boldsymbol{P}_h^{*,k-\frac{1}{2}}}{2} + \delta_\tau \boldsymbol{P}_h^{*,k+\frac{1}{2}} \right) \\ &= -\frac{\tau\mu_0}{4} \sum_{k=0}^{n-1} \left(\sigma^* (\delta_\tau \boldsymbol{E}_h^{k+1} + \delta_\tau \boldsymbol{E}_h^k), \delta_\tau \boldsymbol{P}_h^{*,k+\frac{3}{2}} + \delta_\tau \boldsymbol{P}_h^{*,k-\frac{1}{2}} + 2\delta_\tau \boldsymbol{P}_h^{*,k+\frac{1}{2}} \right) \\ &\leq \frac{\tau\mu_0 C_x^2 \varepsilon_0 \varepsilon_1}{8} \left(\|\delta_\tau \boldsymbol{E}_h^{k+1} + \delta_\tau \boldsymbol{E}_h^k\|_0^2 + \|\delta_\tau \boldsymbol{P}_h^{k+\frac{3}{2}} + \delta_\tau \boldsymbol{P}_h^{k-\frac{1}{2}} + 2\delta_\tau \boldsymbol{P}_h^{k+\frac{1}{2}}\|_0^2 \right) \\ &\leq \frac{\tau\mu_0 C_x^2 \varepsilon_1}{4} \varepsilon_0 \|\delta_\tau \boldsymbol{E}_h^n\|_0^2 + \frac{\tau\mu_0 C_x^2 \varepsilon_1}{2} \sum_{k=0}^{n-1} \varepsilon_0 \|\delta_\tau \boldsymbol{E}_h^k\|_0^2 + \frac{3\tau\varepsilon_0 \varepsilon_1 C_x^2}{8} \mu_0 \|\delta_\tau \boldsymbol{P}_h^{n+\frac{1}{2}}\|_0^2 \\ &\quad + \frac{9\tau\varepsilon_0 C_x^2 \varepsilon_1}{4} \mu_0 \sum_{k=-1}^{n-1} \|\delta_\tau \boldsymbol{P}_h^{k+\frac{1}{2}}\|_0^2, \end{aligned}$$

where we used the impedance matching condition $\frac{\sigma_i}{\varepsilon_0 \varepsilon_1} = \frac{\sigma_{m,i}}{\mu_0}$ $(i = x, y)$, and the fact $\varepsilon_1 \geq 1$.

Now let us consider Err_6. Adding Err_6 and (3.1) with $\phi_h = \tau\mu_0 (\frac{\boldsymbol{P}_h^{*,k+\frac{3}{2}} + \boldsymbol{P}_h^{*,k-\frac{1}{2}}}{2} + \boldsymbol{P}_h^{*,k+\frac{1}{2}})$, we have

$$\begin{aligned} Err_6 &= -\tau\mu_0 \sum_{k=0}^{n-1} \left(\nabla \times \overline{\boldsymbol{P}}_h^{*,k+1}, H_{z,h}^{k+\frac{3}{2}} + H_{z,h}^{k+\frac{1}{2}} \right) \\ &= \tau\mu_0 \sum_{k=0}^{n-1} \left[\left(-\nabla \times \frac{\boldsymbol{P}_h^{*,k+\frac{3}{2}} + \boldsymbol{P}_h^{*,k+\frac{1}{2}}}{2}, H_{z,h}^{k+\frac{3}{2}} \right) + \left(\nabla \times \frac{\boldsymbol{P}_h^{*,k+\frac{1}{2}} + \boldsymbol{P}_h^{*,k-\frac{1}{2}}}{2}, H_{z,h}^{k+\frac{1}{2}} \right) \right] \\ &\quad - \tau\mu_0 \varepsilon_0 \sum_{k=0}^{n-1} \left(\varepsilon_r^* \delta_\tau \boldsymbol{E}_h^{k+1}, \frac{\boldsymbol{P}_h^{*,k+\frac{3}{2}} + \boldsymbol{P}_h^{*,k-\frac{1}{2}}}{2} + \boldsymbol{P}_h^{*,k+\frac{1}{2}} \right) \\ &\quad - \tau\mu_0 \sum_{k=0}^{n-1} \left(\sigma^* \frac{\boldsymbol{E}_h^{k+1} + \boldsymbol{E}_h^k}{2}, \frac{\boldsymbol{P}_h^{*,k+\frac{3}{2}} + \boldsymbol{P}_h^{*,k-\frac{1}{2}}}{2} + \boldsymbol{P}_h^{*,k+\frac{1}{2}} \right) = \sum_{i=4}^{6} rhs_i. \end{aligned}$$

Using $\boldsymbol{P}_h^{n-\frac{1}{2}} = \boldsymbol{P}_h^{n+\frac{1}{2}} - \frac{\tau}{\mu_0}\boldsymbol{E}_h^n$ and the inequality $(\frac{a+b}{2}+c)^2 \le a^2+b^2+2c^2$, we have

$$
\begin{aligned}
rhs_4 &= -\tau\mu_0\left(\nabla\times\frac{\boldsymbol{P}_h^{*,n+\frac{1}{2}}+\boldsymbol{P}_h^{*,n-\frac{1}{2}}}{2}, H_{z,h}^{n+\frac{1}{2}}\right) + \tau\mu_0\left(\nabla\times\frac{\boldsymbol{P}_h^{*,\frac{1}{2}}+\boldsymbol{P}_h^{*,-\frac{1}{2}}}{2}, H_{z,h}^{\frac{1}{2}}\right)\\
&= -\tau\mu_0\left(\nabla\times\boldsymbol{P}_h^{*,n+\frac{1}{2}}, H_{z,h}^{n+\frac{1}{2}}\right) + \frac{\tau^2}{2}\left(\nabla\times\boldsymbol{E}_h^{*,n}, H_{z,h}^{n+\frac{1}{2}}\right) + \frac{\tau\mu_0}{4}\|\nabla\times\boldsymbol{P}_h^{*,\frac{1}{2}}\|_0^2\\
&\quad + \frac{\tau\mu_0}{4}\|\nabla\times\boldsymbol{P}_h^{*,-\frac{1}{2}}\|_0^2 + \frac{\tau\mu_0}{2}\|H_{z,h}^{\frac{1}{2}}\|_0^2\\
&\le \frac{\tau C_{inv}h^{-1}C_x}{2}\left(\mu_0\|\boldsymbol{P}_h^{n+\frac{1}{2}}\|_0^2 + \mu_0\|H_{z,h}^{n+\frac{1}{2}}\|_0^2\right) + \frac{\tau^2 C_{inv}h^{-1}C_xC_v}{4}\left(\varepsilon_0\|\boldsymbol{E}_h^n\|_0^2 + \mu_0\|H_{z,h}^{n+\frac{1}{2}}\|_0^2\right)\\
&\quad + \frac{\tau\mu_0}{4}\|\nabla\times\boldsymbol{P}_h^{*,\frac{1}{2}}\|_0^2 + \frac{\tau\mu_0}{4}\|\nabla\times\boldsymbol{P}_h^{*,-\frac{1}{2}}\|_0^2 + \frac{\tau\mu_0}{2}\|H_{z,h}^{\frac{1}{2}}\|_0^2.
\end{aligned}
$$

Similarly, using the definition of C_x and bounding $\boldsymbol{P}_h^*$ by $\boldsymbol{P}_h$, we easily have

$$
\begin{aligned}
rhs_5 &= -\tau\varepsilon_0\mu_0\sum_{k=0}^{n-1}\left(\varepsilon_r^*\delta_\tau\boldsymbol{E}_h^{k+1}, \frac{\boldsymbol{P}_h^{*,k+\frac{3}{2}}+\boldsymbol{P}_h^{*,k-\frac{1}{2}}}{2} + \boldsymbol{P}_h^{*,k+\frac{1}{2}}\right)\\
&\le \tau\varepsilon_0\mu_0\varepsilon_2C_x\sum_{k=0}^{n-1}\|\delta_\tau\boldsymbol{E}_h^{k+1}\|_0\left\|\frac{\boldsymbol{P}_h^{k+\frac{3}{2}}+\boldsymbol{P}_h^{k-\frac{1}{2}}}{2}+\boldsymbol{P}_h^{k+\frac{1}{2}}\right\|_0\\
&\le \frac{\tau\mu_0\varepsilon_2C_x}{2}\sum_{k=0}^{n}\varepsilon_0\|\delta_\tau\boldsymbol{E}_h^k\|_0^2 + \frac{\tau\varepsilon_0\varepsilon_2C_x}{2}\mu_0\|\boldsymbol{P}_h^{n+\frac{1}{2}}\|_0^2 + \frac{\tau\varepsilon_0\varepsilon_2C_x}{2}\mu_0\|\boldsymbol{P}_h^{-\frac{1}{2}}\|_0^2\\
&\quad + 2\tau\varepsilon_0\varepsilon_2C_x\sum_{k=0}^{n-1}\mu_0\|\boldsymbol{P}_h^{k+\frac{1}{2}}\|_0^2,
\end{aligned}
$$

and

$$
\begin{aligned}
rhs_6 &= -\tau\mu_0\sum_{k=0}^{n-1}\left(\sigma^*\frac{\boldsymbol{E}_h^{k+1}+\boldsymbol{E}_h^k}{2}, \frac{\boldsymbol{P}_h^{*,k+\frac{3}{2}}+\boldsymbol{P}_h^{*,k-\frac{1}{2}}}{2}+\boldsymbol{P}_h^{*,k+\frac{1}{2}}\right)\\
&\le \tau\mu_0\varepsilon_0\varepsilon_1C_x^2\sum_{k=0}^{n-1}\left\|\frac{\boldsymbol{E}_h^{k+1}+\boldsymbol{E}_h^k}{2}\right\|_0\left\|\frac{\boldsymbol{P}_h^{k+\frac{3}{2}}+\boldsymbol{P}_h^{k-\frac{1}{2}}}{2}+\boldsymbol{P}_h^{k+\frac{1}{2}}\right\|_0\\
&\le \frac{\tau\mu_0C_x^2\varepsilon_1}{4}\varepsilon_0\|\boldsymbol{E}_h^n\|_0^2 + \frac{\tau\mu_0C_x^2\varepsilon_1}{2}\sum_{k=0}^{n-1}\varepsilon_0\|\boldsymbol{E}_h^k\|_0^2\\
&\quad + \frac{\tau\varepsilon_0\varepsilon_1C_x^2}{2}\mu_0\|\boldsymbol{P}_h^{n+\frac{1}{2}}\|_0^2 + 2\tau\varepsilon_0\varepsilon_1C_x^2\sum_{k=0}^{n-1}\mu_0\|\boldsymbol{P}_h^{k+\frac{1}{2}}\|_0^2 + \frac{\tau\varepsilon_0\varepsilon_1C_x^2}{2}\cdot\mu_0\|\boldsymbol{P}_h^{-\frac{1}{2}}\|_0^2.
\end{aligned}
$$

The proof is completed by substituting all the above estimates into (3.17) with the choice of time step τ satisfying the constraint (3.6), and $\delta_1 = \frac{\varepsilon_1}{6\varepsilon_2}$ so that all terms can be controlled by the left hand side terms, and then by using the discrete Gronwall inequality. □

4. Simulation of optical black holes

In this section, we provide three examples showing the effectiveness of our FETD method. The cylindrical, elliptical and square optical black holes are simulated.

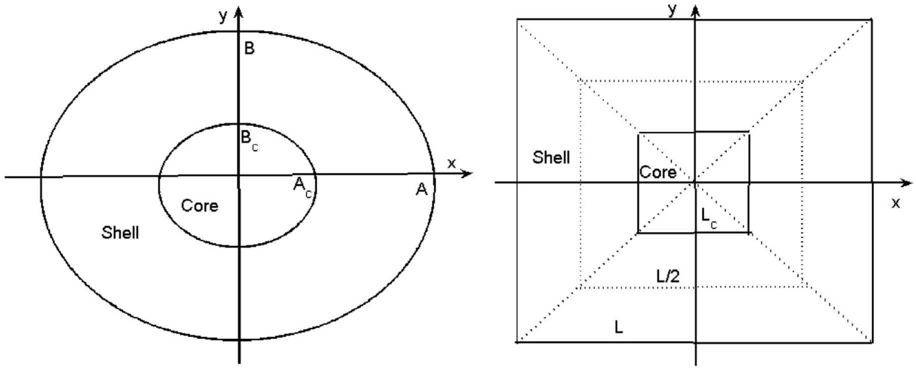

Fig. 4.1. Illustration of the elliptical and square OBHs.

Recall that the relative electric permittivity for the cylindrical optical black hole is given by (2.5). The relative electric permittivity of the elliptical black hole (cf. Fig. 4.1) can be constructed similarly to the cylindrical black hole:

$$\varepsilon_r(r) = \begin{cases} \varepsilon_1, & x^2 + k^2y^2 > A^2, \\ \varepsilon_1 \left(\dfrac{A^2}{x^2 + k^2y^2}\right)^{\frac{n}{2}}, & A_c^2 \le x^2 + k^2y^2 \le A^2 \\ \varepsilon_2 + i\gamma & x^2 + k^2y^2 < A_c^2, \end{cases} \tag{4.1}$$

where $k = \frac{A}{B} = \frac{A_c}{B_c}$ denotes the axis ratio.

The relative electric permittivity of a square OBH was developed in [33]:

$$\varepsilon_r(r) = \begin{cases} \varepsilon_1, & |x| > \dfrac{L}{2} \text{ or } |y| > \dfrac{L}{2}, \\ \varepsilon_1 \left(\dfrac{L}{2|x|}\right)^n, & \dfrac{L_c}{2} \le |x| \le \dfrac{L}{2} \text{ and } |x| \ge |y| \\ \varepsilon_1 \left(\dfrac{L}{2|y|}\right)^n, & \dfrac{L_c}{2} \le |y| \le \dfrac{L}{2} \text{ and } |x| < |y| \\ \varepsilon_2 + i\gamma, & |x| < \dfrac{L_c}{2} \text{ and } |y| < \dfrac{L_c}{2}. \end{cases} \tag{4.2}$$

In all the simulations, the incident source wave is imposed as component $H_z = 0.1sin(\omega t)$, the parameter $n = 2$ is fixed, and a PML with 12 cells in each direction around the physical domain is used.

Example 1 (*Cylindrical OBHs*)**.** In this example, we consider that the cylindrical black hole is embedded in SiO_2 (which has electric permittivity $\varepsilon_1 = 2.1$), and the core of the device is composed of n-doped silicon with electric permittivity $\varepsilon_2 + i\gamma = 12 + 0.7i$. The physical domain is chosen to be $[0, 45]$ µm × $[0, 45]$ µm, and the physical parameters $R_c = 8.4$ µm (micrometer), $R_{sh} = R_c\sqrt{\frac{\varepsilon_2}{\varepsilon_1}}$. The computational mesh is obtained by uniformly refining the coarse mesh given in Fig. 4.2 five times, and the time step is chosen as $\tau = 2.5 \cdot 10^{-17}$ s, and the center frequency is $f = 100$ THz.

To see how wave propagates in the black hole, we simulated two cases: Case 1 with the incident source wave located at $x = 0$, $y \in [37.6, 41.5]$ µm; Case 2 with the incident source wave located at $x = 0$, $y \in [22.5, 25]$ µm. In Figs. 4.3 and 4.4, we plot the calculated magnetic fields H_z at different time steps. In both cases, it is clear that the electromagnetic waves bend rapidly toward the core of the black hole, and the waves are totally absorbed inside the core of the device (cf. Figs. 4.3 and 4.4). Furthermore, we can easily see that there is almost no reflection, since the device is designed to match the surrounding material. We like to remark that our results are similar to those obtained by the FDTD method [9].

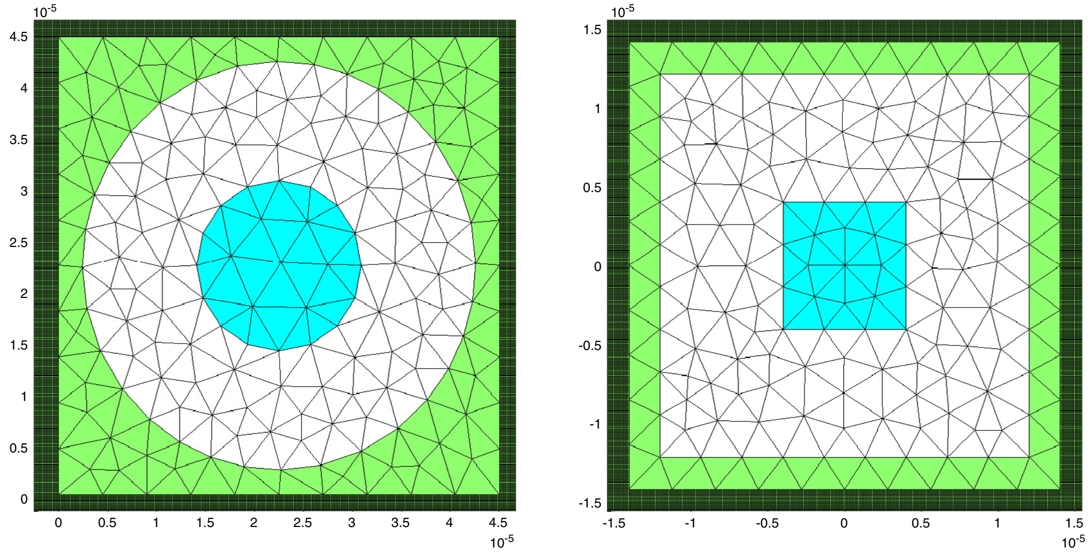

Fig. 4.2. The sample coarse meshes for cylindrical and square OBHs (the real meshes used in our simulations are obtained by uniformly refining the triangular elements five times).

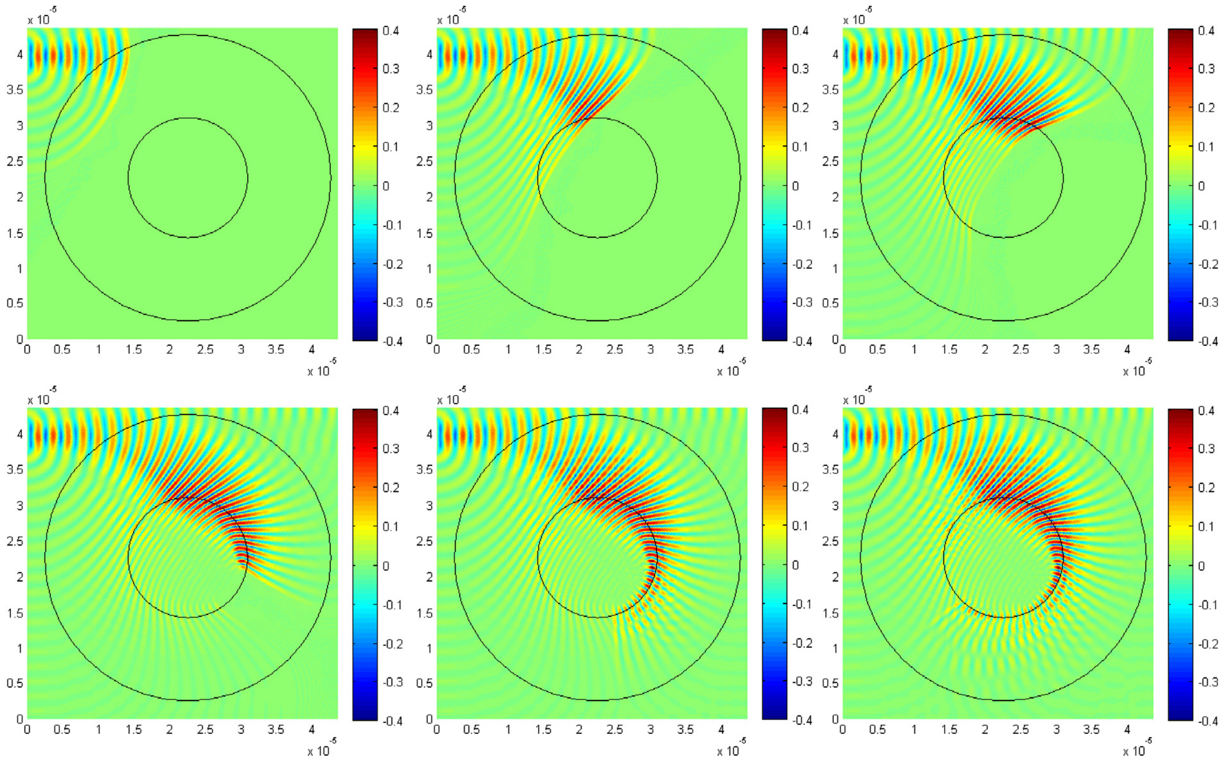

Fig. 4.3. Case 1 of Example 1. Magnetic fields H_z at various time steps for the cylindrical OBHs simulation. Top left: 2800 steps. Top middle: 6000 steps. Top right: 8000 steps. Bottom left: 12,000 steps. Bottom middle: 16,000 steps. Bottom right: 20,000 steps.

Example 2 (*Elliptical OBHs*)**.** In this example, we simulate the elliptical optical black hole by our FETD method. The elliptical black hole is embedded in vacuum, in other words the relative electric permittivity $\varepsilon_1 = 1$. The physical domain is chosen to be $[-15, 15]$ μm × $[-20, 20]$ μm, and the physical parameters in (4.1) are $A = 2$ μm, $B = 8$ μm, $\varepsilon_2 = 16$, and $k = \frac{1}{2}$. The time step is chosen as $\tau = 3 \cdot 10^{-17}$ s, and the center frequency is $f = 150$ THz. There

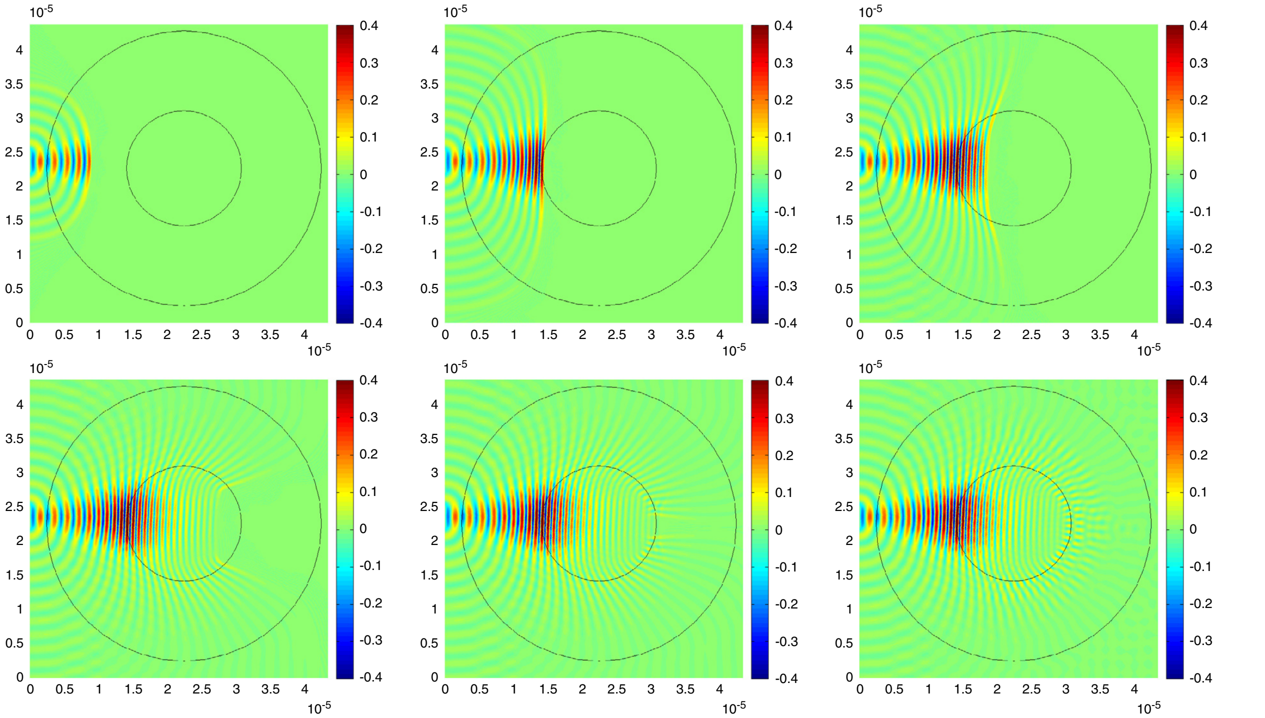

Fig. 4.4. Case 2 of Example 1. Magnetic fields H_z at various time steps for the cylindrical OBHs simulation. Top left: 2000 steps. Top middle: 4000 steps. Top right: 6000 steps. Bottom left: 10,000 steps. Bottom middle: 12,000 steps. Bottom right: 20,000 steps.

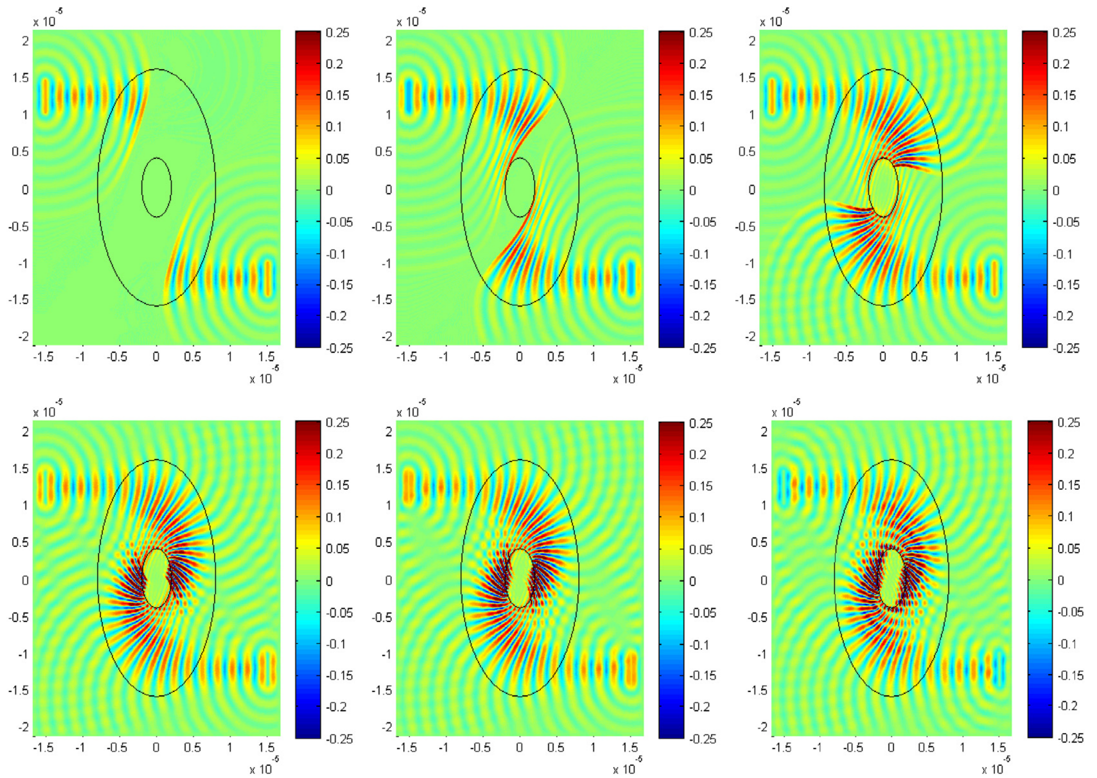

Fig. 4.5. Example 2. Magnetic fields H_z at various time steps for the elliptical OBHs simulation. Top left: 1600 steps. Top middle: 2400 steps. Top right: 3600 steps. Bottom left: 4800 steps. Bottom middle: 5200 steps. Bottom right: 8000 steps.

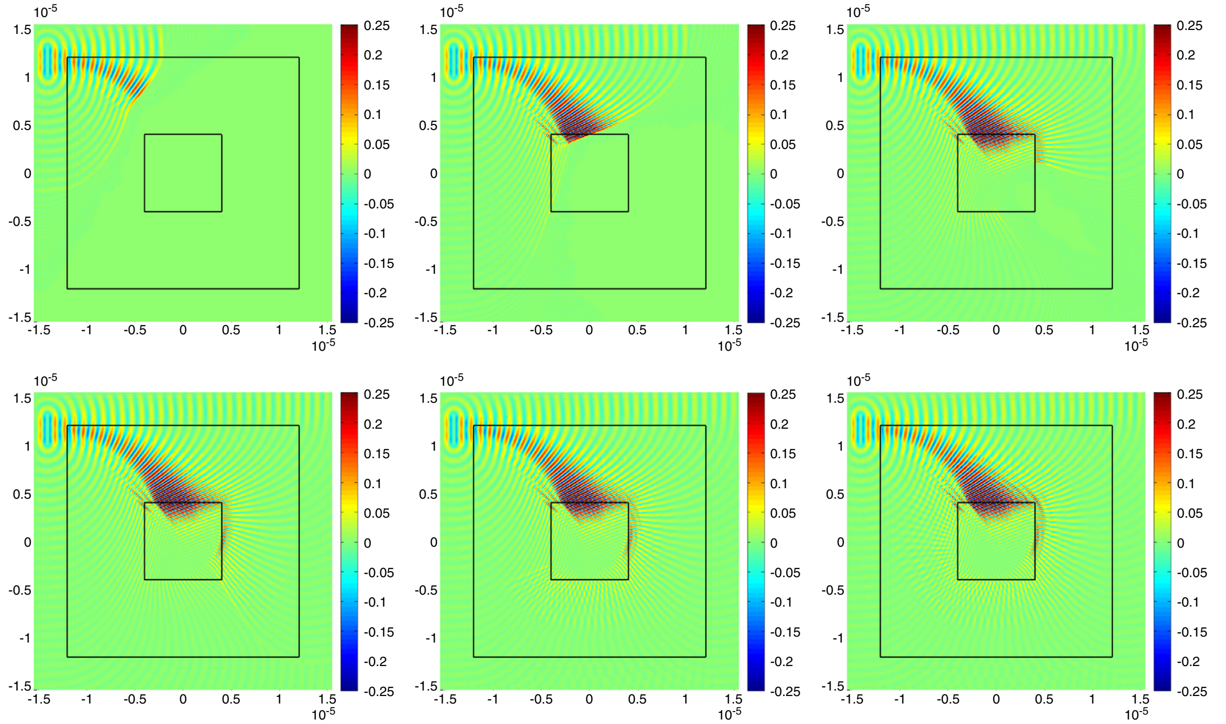

Fig. 4.6. Case 1 of Example 3. Magnetic fields H_z at various time steps for the square OBHs simulation. Top left: 1000 steps. Top middle: 2000 steps. Top right: 3000 steps. Bottom left: 4000 steps. Bottom middle: 6000 steps. Bottom right: 10,000 steps.

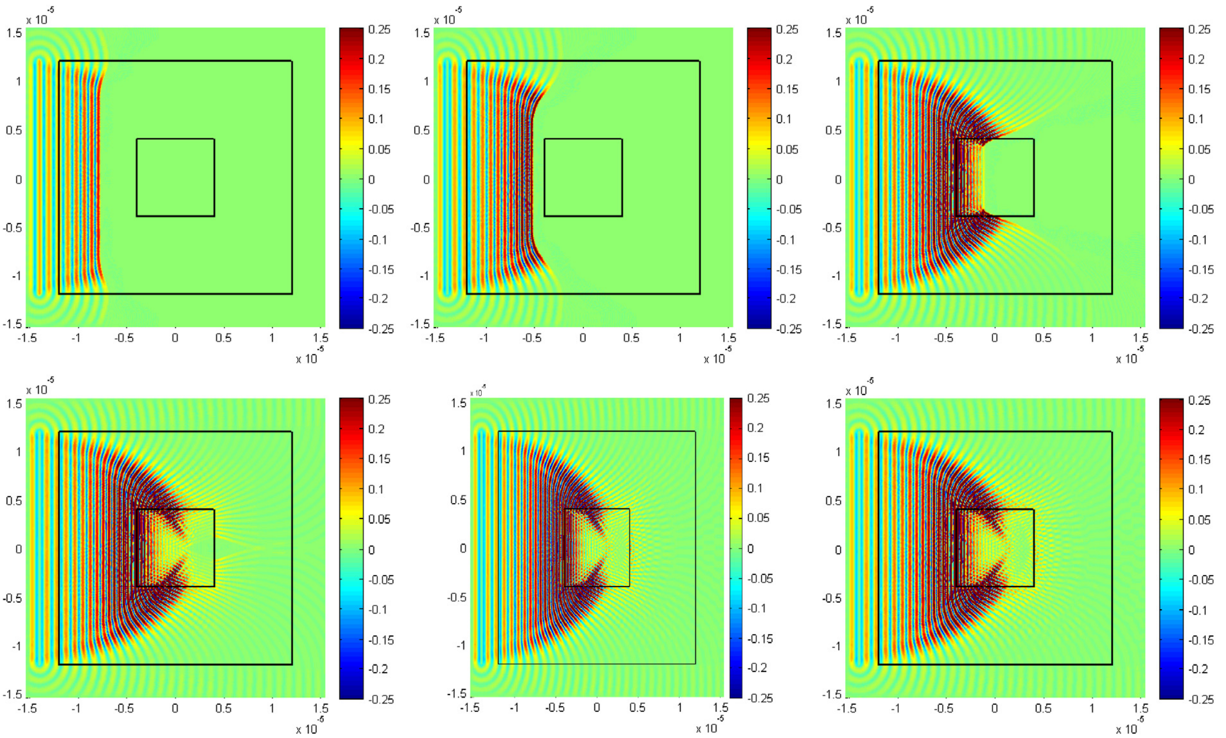

Fig. 4.7. Case 2 of Example 3. Magnetic fields H_z at various time steps for the square OBHs simulation. Top left: 500 steps. Top middle: 1000 steps. Top right: 2000 steps. Bottom left: 3000 steps. Bottom middle: 4000 steps. Bottom right: 10,000 steps.

are two incident source waves in this simulation: one is located at $x = -15$ μm, $y \in [10, 14.5]$ μm, and the other one is located at $x = 1.5$, $y \in [-14.5, -10]$ μm. The calculated magnetic fields H_z at various time steps are plotted in Fig. 4.5, which shows that the two waves also rapidly bend toward the core of the device, and are totally absorbed by the core. From this simulation, we can see that the optical black hole can absorb the electromagnetic waves radiating from different locations.

Example 3 (*Square OBHs*). In this example, we consider the square optical black hole. The physical domain is chosen to be $[-15\ \mu\text{m}, 15\ \mu\text{m}]^2$, the core domain is $[-4\ \mu\text{m}, 4\ \mu\text{m}]^2$, and the shell domain is $[-12\ \mu\text{m}, 12\ \mu\text{m}]^2 \setminus [-4\ \mu\text{m}, 4\ \mu\text{m}]^2$. The physical parameters $\varepsilon_2 = 9, \gamma = 0.7$. The time step is chosen as $\tau = 4 \cdot 10^{-17}$ s, and the center frequency is $f = 300$ THz. We simulated two types of incident source waves in this example. In Case 1, the source wave is generated by a Gaussian wave and located at $x = -14$ μm, $y \in [10\ \mu\text{m}, 13.125\ \mu\text{m}]$. While in Case 2, the second source wave is a plane wave located at $x = -14$ μm, $y \in [-12\ \mu\text{m}, 12\ \mu\text{m}]$. We present the calculated magnetic fields H_z at different time steps in Figs. 4.6 and 4.7, which have the similar wave propagation pattern as Figs. 4.3–4.5. From Figs. 4.6 and 4.7, we can see that the optical black hole can effectively absorb these two types of electromagnetic waves, and there is no reflection in both cases.

5. Conclusions

In this paper, we study the mathematical formulation of optical black holes (OBHs). A finite element time domain (FETD) method is designed to simulate OBHs, and the stability of our FETD method is established. Numerical simulations of the cylindrical, elliptical and square OBHs are performed. Our numerical results demonstrate that our FETD method is an effective tool for simulating OBHs in addition to the FDTD method.

References

[1] A. Greenleaf, Y. Kurylev, M. Lassas, G. Uhlmann, Cloaking devices, electromagnetics wormholes and transformation optics, SIAM Rev. 51 (2009) 3–33.

[2] R.V. Kohn, D. Onofrei, M.S. Vogelius, M.I. Weinstein, Cloaking via change of variables for the Helmholtz equation, Comm. Pure Appl. Math. 63 (2010) 0973–1016.

[3] E.E. Narimanov, A.V. Kildishev, Optical black hole: Broadband omnidirectional light absorber, Appl. Phys. Lett. 95 (2009) 041106.

[4] N. Engheta, R.W. Ziolkowski, Electromagnetic Metamaterials: Physics and Engineering Explorations, Wiley IEEE Press, 2006.

[5] P. Markos, C.M. Soukoulis, Wave Propagation: From Electrons to Photonic Crystals and Left-Handed Materials, Princeton University Press, 2008.

[6] G. Shvets, I. Tsukerman, Plasmonics and Plasmonic Metamaterials: Analysis and Applications, World Scientific, 2012.

[7] J. Li, Y. Huang, Time-Domain Finite Element Methods for Maxwell's Equations in Metamaterials, in: Springer Ser. Comput. Math., vol. 43, Springer, New York, 2013.

[8] Y. Hao, R. Mittra, FDTD Modeling of Metamaterials: Theory and Applications, Artech House Publishers, 2008.

[9] C. Argyropoulos, E. Kallos, Y. Hao, FDTD analysis of the optical black hole, JOSAB 27 (2010) 2020–2025.

[10] J. Qiu, H.L. Liu, P.F. Hsu, Radiative properties of optical board embedded with optical black holes, J. Quant. Spectrosc. Radiat. Transfer 112 (2011) 832–838.

[11] S. Zhao, G.W. Wei, High-order FDTD methods via derivative matching for Maxwell's equations with material interface, J. Comput. Phys. 200 (2004) 60–103.

[12] M. Ainsworth, J. Coyle, Hierarchic hp-edge element families for Maxwell's equations on hybrid quadrilateral/triangular meshes, Comput. Methods Appl. Mech. Engrg. 190 (2001) 6709–6733.

[13] H.T. Banks, V.A. Bokil, N.L. Gibson, Analysis of stability and dispersion in a finite element method for Debye and Lorentz media, Numer. Methods Partial Differ. Equ. 25 (2009) 885–917.

[14] G. Bao, P. Li, H. Wu, An adaptive edge element method with perfectly matched absorbing layers for wave scattering by biperiodic structures, Math. Comput. 79 (2010) 1–34.

[15] R. Beck, R. Hiptmair, H.W. Hoppe, B. Wohlmuth, Residual based a posteriori error estimators for eddy current computation, Math. Model. Numer. Anal. 34 (2000) 159–182.

[16] A.-S. Bonnet-Ben Dhia, L. Chesnel, P. Ciarlet Jr., Two-dimensional Maxwell's equations with sign-changing coefficients, Appl. Numer. Math. 79 (2014) 29–41.

[17] S.C. Brenner, F. Li, L.-Y. Sung, A locally divergence-free nonconforming finite element method for the time-harmonic Maxwell equations, Math. Comput. 76 (2007) 573–595.

[18] A. Buffa, I. Perugia, T. Warburton, The mortar-discontinuous Galerkin method for the 2D Maxwell eigenproblem, J. Sci. Comput. 40 (2009) 86–114.

[19] Z. Chen, Q. Du, J. Zou, Finite element methods with matching and non-matching meshes for Maxwell's equations with discontinuous coefficients, SIAM J. Numer. Anal. 37 (2000) 1542–1570.

[20] S. Jund, S. Salmon, E. Sonnendrücker, High-order low dissipation conforming finite-element discretization of the Maxwell equations, Commun. Comput. Phys. 11 (2012) 863–892.

[21] Z. Qiao, C. Yao, S. Jia, Superconvergence and extrapolation analysis of a nonconforming mixed finite element approximation for time-harmonic Maxwell's equations, J. Sci. Comput. 46 (2011) 1–19.

[22] R.N. Rieben, G.H. Rodrigue, D.A. White, A high order mixed vector finite element method for solving the time dependent Maxwell equations on unstructured grids, J. Comput. Phys. 204 (2005) 490–519.

[23] C. Scheid, S. Lanteri, Convergence of a discontinuous Galerkin scheme for the mixed time domain Maxwell's equations in dispersive media, IMA J Numer. Anal. 33 (2013) 432–459.

[24] Y. Zhang, L.-Q. Cao, Y.-S. Wong, Multiscale computations for 3D time-dependent Maxwell's equations in composite materials, SIAM J. Sci. Comput. 32 (2010) 2560–2583.

[25] L. Demkowicz, Computing with hp-adaptive finite elements, in: One and Two Dimensional Elliptic and Maxwell Problems, Computing with hp-Adaptive Finite Elements, vol. 1, CRC Press, Taylor and Francis, 2007.

[26] L. Demkowicz, J. Kurtz, D. Pardo, M. Paszynski, W. Rachowicz, A. Zdunek, Computing with hp-Adaptive Finite Elements. vol. 2: Frontiers: Three Dimensional Elliptic and Maxwell Problems with Applications, CRC Press, Taylor and Francis, 2008.

[27] J.S. Hesthaven, T. Warburton, Nodal Discontinuous Galerkin Methods: Algorithms, Analysis, and Applications, Springer, New York, 2008.

[28] P. Monk, Finite Element Methods for Maxwell's Equations, Oxford University Press, Oxford, 2003.

[29] Y. Huang, J. Li, W. Yang, Modeling backward wave propagation in matamaterials by the finite element time domain method, SIAM J. Sci. Comput. 35 (2013) B248–B274.

[30] J. Li, Numerical convergence and physical fidelity analysis for Maxwell's equations in metamaterials, Comput. Methods Appl. Mech. Engrg. 198 (2009) 3161–3172.

[31] J.P. Berenger, A perfectly matched layer for the absorption of electromagnetic waves, J. Comput. Phys. 114 (1994) 185–200.

[32] E. Turkel, A. Yefet, Absorbing PML boundary layers for wave-like equations, Appl. Numer. Math. 27 (1998) 533–557.

[33] J. Qiu, J.Y. Tan, L.H. Liu, P.F. Hsu, Infrared radiative properties of two-dimensional square optical black holes, J. Quant. Spectrosc. Radiat. Transfer 112 (2011) 2584–2591.